Chemical Engineering Journal Advances 18 (2024) 100602

Contents lists available at ScienceDirect

Chemical Engineering Journal Advances

journal homepage: www.sciencedirect.com/journal/chemical-engineering-journal-advances

# Optimizing levofloxacin decontamination in aquatic environment: Iron-modified biochar in heterogeneous Fenton processes with peroxide and persulfate

Antonio Faggiano [a,b], Oriana Motta [b,c], Maurizio Carotenuto [a], Maria Ricciardi [a,b], Antonino Fiorentino [a,b,*], Antonio Proto [a,b]

[a] Department of Chemistry and Biology "Adolfo Zambelli", University of Salerno, via Giovanni Paolo II 132, 84084 Fisciano, SA, Italy
[b] National Interuniversity Consortium of Materials Science and Technology (INSTM), 50121 Firenze, FI, Italy
[c] Department of Medicine Surgery and Dentistry "Scuola Medica Salernitana", University of Salerno, via S. Allende 1, 84081 Baronissi, SA, Italy

ARTICLE INFO

*Keywords:*
Functionalized biochar
Heterogeneous Fenton process
Chemometrics approach
Water treatment
Antibiotics removal

ABSTRACT

This study evaluates the effectiveness of iron-modified biochar (Fe-BC) in fixed-bed heterogeneous Fenton processes for levofloxacin (LFX) removal, a widely-used fluoroquinolone antibiotic. The objective is to optimize parameters such as pH, oxidants ($H_2O_2$ and $S_2O_8^{2-}$), and biochar forms (functionalized and raw) using factorial analysis of mixed data (FAMD) and response surface methodology (RSM). These optimizations identified the ideal conditions for maximal LFX removal. The most effective removal with Fe-BC occurred at 2.5 mM $H_2O_2$ and pH 7.5, while the optimal $S_2O_8^{2-}$ conditions were 1.6 mM at pH 2.8. Both Fe-BC and raw biochar (RBC) showed the highest adsorption at pH 5.8. In adsorption-only, RBC and Fe-BC reduced LFX to 530 μg/L and 335 μg/L, respectively, in 60 min. The oxidation process further decreased LFX levels to between 8.9 μg/L and 0.1 μg/L using $S_2O_8^{2-}$ and $H_2O_2$, respectively. The research expanded upon a kinetic model, incorporating the calculation of kinetic constants for both adsorption and oxidation processes, to deepen our understanding of the intricate degradation dynamics at play. Identifying by-products was crucial in elucidating degradation pathways. These findings are vital for environmental remediation, demonstrating the efficiency of Fe-BC in removing harmful antibiotics from water. This research highlights the potential of modified biochar in environmental clean-up, especially for water contaminated with antibiotics. The results emphasize the importance of optimizing treatment conditions for effective antibiotic removal, contributing valuable insights to the field of environmental remediation.

## 1. Introduction

In recent times, there has been a notable rise in the utilization of antibiotics, both in the field of human health and within intensive livestock farming. Consequently, this surge in antibiotic usage has resulted in an escalation of the concentration of these drugs in wastewater effluents [1]. The emergence of antibiotic-resistant bacteria has become a significant public health concern due to the excessive use of antibiotics. The release of antibiotics into the environment through wastewater effluents can further aggravate the spread of antibiotic resistance. Urban wastewater treatment plants (WWTPs) have emerged as one of the primary sources responsible for the release of antibiotics into various environmental compartments on a global scale [2]. LFX, classified as a FQ antibiotic, is widely employed due to its effectiveness [3]. In light of the COVID-19 pandemic, several therapeutic approaches have been developed, with LFX being identified as a potent inhibitor of SARS-CoV-2 replication through its interaction with the main binding protease [4]. Similar to other FQs, LFX exhibits significant resistance to conventional biological oxidation and is typically discharged into the environment via WWTPs [5]. FQs, are prevalent antibiotics that enter

*Abbreviations:* FAMD, factorial analysis of mixed data; Fe-BC, iron-modified biochar; FQs, fluoroquinolones antibiotics; FTIR, Fourier transform infrared spectroscopy; LFX, levofloxacin; PFO, pseudo-first order; PSO, pseudo-second order; RBC, raw biochar; RMSE, root mean square error; RSM, response surface methodology; WWTP, wastewater treatment plant; XRD, X-ray diffraction.

* Corresponding author.
*E-mail address:* afiorentino@unisa.it (A. Fiorentino).

https://doi.org/10.1016/j.ceja.2024.100602

Available online 8 April 2024

the environment through pharmaceutical discharge, agricultural runoff, and improper disposal, posing significant ecological and public health challenges. Their transport and behaviour in ecosystems are influenced by physicochemical properties, adsorption to organic and mineral substrates, and interactions with environmental factors like pH and divalent cations, which affect their mobility. The persistence of FQs, coupled with their bioaccumulative potential, risks biomagnification across trophic levels and fosters the development of antibiotic-resistant bacterial strains. This selective pressure on microbial communities leads to the dissemination of resistance, disrupting natural ecosystems and complicating treatment options for infections [6–9]. The concentration of LFX in natural waters and wastewater exhibits a significant variance, with reported values spanning from ng/L to mg/L. For instance, concentrations in river water and wastewater in Kenya were found to be 0.04 μg/L and 1.60 μg/L, respectively, while in Nigeria, hospital effluents contained LFX levels ranging from 0.1 to 0.3 mg/L. Further afield, wastewater streams in Pakistan and India showed even higher concentrations, at 6.63 mg/L and 0.54 mg/L respectively, underscoring the broad spectrum of LFX prevalence in aquatic environments [10]. To mitigate the dissemination of antibiotics in the environment and water bodies, numerous innovative techniques have been reported for the degradation of these substances in water matrices. Notably, adsorption, photocatalysis, and advanced oxidation processes (AOPs) have shown great promise [11,12]. AOPs have been extensively investigated in recent decades and can be employed as either the primary or final step in water and wastewater treatment processes [13]. Hydroxyl radical-based homogeneous and heterogeneous Fenton and Fenton-like processes have been the subject of extensive research for the degradation of FQs in wastewater in recent years [14–17]. While $H_2O_2$ has traditionally been the most commonly used oxidizing agent in Fenton processes, there has been a growing interest in exploring $S_2O_8^{2-}$ as an alternative oxidant for the decontamination of water and wastewater from emerging contaminants such as antibiotics [18–21]. Among the various AOPs, the heterogenous Fenton process utilizing metal catalysts supported on carbonaceous materials with either $H_2O_2$ or $S_2O_8^{2-}$ is emerging as a promising technology for the degradation of FQs [15,16,22]. Recently, investigations have been conducted on biochar (BC)-based iron materials as activators of Fenton processes. These materials have shown the ability to enhance the formation of $SO4^{\bullet-}$ and •OH radicals, surpassing the capabilities of conventional activators [23–25]. BC has gained significant attention in the scientific community due to its status as a secondary raw material derived from the biomass pyrolysis process. In addition to its use as a soil conditioner, BC has proven to be an effective and affordable adsorbent for both organic and inorganic contaminants [26]. Recent studies have unveiled the potential of BC in facilitating hydroxyl and sulphate radical based heterogeneous AOPs. This is attributed to its high surface area, porous structure, and abundance of active oxygen-containing functional groups, such as carboxylic and hydroxyl groups. BC has demonstrated the capability to activate $H_2O_2$ and $S_2O_8^{2-}$ and support metals and metal oxides catalysts in the Fenton process [27–29]. The utilization of $S_2O_8^{2-}$ instead of $H_2O_2$ offers several advantages, as $SO4^{\bullet-}$ radicals possess a higher redox potential (2.5–3.1 V) compared to $^{\bullet}OH$ (1.8–2.7 V). Consequently, they exhibit greater selectivity for the oxidation reaction and a longer half-life period (t1/2 = 30–40 μs versus 20 ns) [30,31]. Heterogeneous technologies also present advantages over homogeneous ones. In homogeneous Fenton processes, the use of Fe(II) and Fe(III) salts results in a significant drawback, namely the production of a substantial amount of iron sludge during water treatment. To address this issue, supported-metal heterogeneous catalysts have been developed in recent decades [32]. Among these materials, metal-impregnated biochar shows promise as a potential Fenton catalyst at an industrial scale. However, further efforts are required to design compact and simplified reactors [27]. Previous studies have primarily focused on investigating the utilization of modified BC as Fenton catalysts in batch experiments [33–35], employing a specific quantity of suspended BC catalyst. Further research is needed to optimize the use of advanced oxidation processes for the degradation of antibiotics in wastewater. This includes investigating the use of different catalysts and oxidants, as well as developing more efficient and cost-effective treatment processes [27].

The objective of this study is to explore the ideal parameters within the fixed-bed heterogeneous Fenton process, utilizing biochar functionalized with the aid of $H_2O_2$ and $S_2O_8^{2-}$, to effectively remove LFX from contaminated water. This research marks the first time that biochar, specifically raw biochar (RBC) and iron-modified biochar (Fe-BC), has been applied as Fenton catalysts in such a context, and includes a critical evaluation to determine the more effective oxidant of the two. The novelty of the chemometrics approach applied lies in the application of Response Surface Methodology (RSM) and Factorial Analysis of Mixed Data (FAMD) not only to optimize the process but also to streamline it, ensuring that it is scalable for widespread application. Our experimental design utilizes a two-level factorial framework in conjunction with RSM, focusing on key operational variables such as oxidant concentration, treatment duration, pH levels, and the type of catalyst. These factors were meticulously calibrated to target the efficient elimination of LFX. The adoption of a cubic model for each response, coupled with the generation of contour plots and three-dimensional response surfaces, provides a comprehensive visualization of the process optimization. In this research, particular attention was given to the mathematical representation and quantification of reaction rates within the fixed-bed heterogeneous Fenton process, especially focusing on the adsorption processes and the chemical oxidation reactions facilitated by $S_2O_8^{2-}$ and $H_2O_2$. Through rigorous experimental design and analysis, kinetic constants (k values) were meticulously calculated for both the adsorption process and the oxidation reactions. This approach underscores a gap in current scientific literature, where such detailed exploration of kinetic constants in these specific processes remains relatively uncharted. The meticulous calculation of these constants not only provides a foundation for further research but also highlights the necessity for more in-depth studies in this area to fully understand the dynamics and mechanisms at play. Additionally, this research delves into the degradation pathways of LFX to enhance our understanding of the biochemical impacts resulting from the oxidation process. This study not only aims to achieve minimal LFX concentrations but also aspires to set a new benchmark for the implementation of advanced oxidation processes in water treatment technologies.

## 2. Materials and methods

### 2.1. Chemicals

Iron(II) sulphate heptaydrate ($FeSO_4•7H_2O$), hydrogen peroxide ($H_2O_2$) 30% wt, potassium persulfate ($K_2S_2O_8$), sulfuric acid ($H_2SO_4$) 98 %, potassium hydrogen phthalate ($C_8H_5KO_4$), silver sulphate ($Ag_2SO_4$), potassium dichromate ($K_2Cr_2O_7$), mercury sulphate ($HgSO_4$), ethanol (EtOH, >99 %) and tert-butyl alcohol (TBA, >99.5 %) and sodium hydroxide (NaOH) were purchased from Sigma Aldrich (Saint Louis, MO, USA) and used without further purification. RBC was procured from " RESET S.P.A." (Rome, Italy).

### 2.2. Experimental design

In this study, RSM was used for the experimental design of the heterogeneous Fenton processes. Oxidant concentration ($X_1$), treatment time ($X_2$) and initial solution pH ($X_3$) were selected as numerical factors while catalyst type (BC or Fe-BC) ($X_4$) and the type of oxidant ($H_2O_2$ or $S_2O_8^{2-}$) ($X_5$) were selected as categorical factor. LFX degradation (%) was selected as target response. The experimental design involved 137 runs, based on a two-level central composite design (CCD). Each parameter was coded as − 1 (minimum), 0 (medium), +1 (maximum), +α and -α. In this work α=1.682. The ranges and levels for each factor are provided in Table 1. The rationale for the range and levels chosen for each factor,

**Table 1**
Ranges and levels for each factor.

| Variables | Code | Range and levels | | | | | | |
|---|---|---|---|---|---|---|---|---|
| | | L1 | L2 | L3 | L4 | L5 | L6 | L7 |
| Oxidant concentration (mM) | $X_1$ | – | – | 0 | 0.7 | 1.6 | 2.5 | – |
| Time (min) | $X_2$ | 2 | 5 | 15 | 20 | 30 | 50 | 60 |
| pH | $X_3$ | – | 2.8 | 4 | 5.8 | 7.5 | 8.5 | – |
| Oxidant type | $X_4$ | – | – | $H_2O_2$ | $S_2O_8^{2-}$ | – | – | – |
| Catalyst type | $X_5$ | – | – | BC | Fe-BC | – | – | – |

detailed in Table 1, originates from a thorough review of existing literature, preliminary experiments, and the need to encompass a wide yet relevant spectrum of conditions for the Fenton reaction. For instance, the oxidant concentration and treatment time were assigned multiple levels to finely dissect their influence on LFX degradation. Conversely, the initial solution pH, a crucial but more precisely influential variable, was assessed across five levels to capture its optimal range without overcomplicating the design. The oxidant type and catalyst type were categorized simplistically to directly compare the effects of these fundamental variations in the Fenton process. The entire RSM design is presented in Table SM1 of supporting material file (SM).

The removal efficiencies, for all the parameters, were calculated according to the following equation (Eq. 1) [36]:

$$R_{\%} = \frac{C_0 - C_t}{C_0} \times 100 \quad (1)$$

Where:

$R_{\%}$= percentage removal;
$C_0$= concentration at time zero;
$C_t$= concentration at time t.
The response was estimated through a cubic model according to the Eq. 2:

$$Y = b_0 + \sum_{i=1}^{n} b_i X_i + \sum_{i=1}^{n} b_{ii} X_i^2 + \sum_{i=1}^{n-1} \sum_{j=1+1}^{n} b_{ij} X_i X_j + \varepsilon \quad (2)$$

Y is the response of LFX removal, $b_0$ is a constant, $b_i$ correspond to linear coefficient of $X_i$, $b_{ii}$ is the second order effect on regression coefficients, $b_{ij}$ is the interaction coefficient and $\varepsilon$ is the statistical error. After the calculation of the optimal process in terms of type of oxidant, oxidant dose, pH and treatment time and three replicates of this process were made and the kinetic of LFX removal was calculated. For the optimization of the process, the minimization of treatment time was evaluated while no conditions were set for the other factors to assess the process in its entirety. The minimization was selected as goal for final LFX concentration response. All the processes at the optimized conditions were repeated in triplicate.

### 2.3. Fe-BC preparation

The functionalization was made adapting the post-pyrolysis method reported in literature [37–41]. Firstly, the BC was treated with a 15 % $H_2O_2$ solution to augment the oxygen-containing surface functional groups at 25 °C for 24 h. After the oven-drying at 120 °C, Fe-BC was prepared through direct hydrolysis of iron salt following the reaction (Eq.3):

$$FeCl_3 \cdot 6H_2O \rightarrow Fe(OH)_3 + 3HCl + 3H_2O \quad (3)$$

Solutions of iron salt, prepared by dissolving 8 g of $FeCl_3 \cdot 6\ H_2O$ in 50 ml of deionized water, were mixed with 10 g of biochar for 12 h under continuous strong agitation using a magnetic stirrer, and then dried at 200–250 °C to allow the chlorides to be driven off as HCl and $Cl_2$ gas and convert the metal ions to metal oxides.

### 2.4. Biochar characterization

Fourier Transform Infrared Spectroscopy (FTIR) spectra of RBC and Fe-BC were acquired using a Bruker Vertex70 spectrometer. To prepare the samples, a mixture of the powdered sample and FTIR-grade KBr was utilized to form potassium bromide disks. These disks were used for transmittance mode measurements in the spectral range of 600–4000 $cm^{-1}$, with a resolution of 4 $cm^{-1}$. Before spectral acquisition, all samples were finely ground. The collected spectra were presented in Transmittance units. X-ray diffraction (XRD) analyses on the materials were performed using a Bruker D2 Advance automatic diffractometer with nickel-filtered CuKα radiation. Data were recorded in the 2θ range of 10–70° with a resolution of 0.02°

### 2.5. Experimental set-up

The experiments were conducted in continuous-flow recirculation mode. The experimental set-up consisted of two Pyrex glass columns packed one with 16 g of BC and one with 16 g of Fe-BC, the quantity needed to fill all the column (Fig. 1). Each column had an internal diameter of 2.5 cm and a length of 40 cm. Prior to start the flow, the pH was adjusted to the desired value and the oxidant dose was added under stirring. LFX solution was transferred from the feed tanks to the oxidation columns through a two-channel peristaltic pump. After 1 min from oxidant adding, the pump was turned on and the process was started. For each test 1 L of LFX solution (25 mg/L) was treated. The flow was set to 80 mL/min. The scavenging tests for optimized processes were performed based on the optimized parameters. EtOH was employed as quencher for both $SO_4^{\bullet-}$ and $^{\bullet}OH$, while TBA effectively quenched $^{\bullet}OH$ but not $SO_4^{\bullet-}$. The alchols/oxidant molar ratios employed were 1/1 and 1/20 to better understand the species formed, and their behaviour, in each process [42,43]. Specifically, in the Fe-BC/$H_2O_2$ experiments two concentrations of each alcohol (EtOH and TBA) were employed (2.5 mM and 50 mM), while 1.6 mM and 30 mM of each alcohol were employed in Fe-BC/$S_2O_8^{2-}$ experiments.

### 2.6. Analytical measurements

#### 2.6.1. LFX and by-products determination

LFX concentration was evaluated with High Performance Liquid Chromatography Diode Array Detector (HPLC-DAD) analysis through an UltiMate 3000 system (Thermo Fisher Scientific, Waltham, MA USA), equipped with binary pump, automatic sample injector with 100 µL loop and column thermostat. Reversed-phase column (Luna 5µ, 150 mm x 4.6 mm i.d., pore size of 5 µm, Phenomenex) was used for chromatographic separation at 25 °C. The analysis was performed in isocratic mode. Mobile phase consisted of acetonitrile/water:70/30 v/v, a flow rate of 1 mL/min and a detection wavelength of 298 nm were used for the chromatographic separations. This wavelength corresponds to the maximum absorption of LFX. Calibration curves for LFX were prepared by diluting LFX with acetonitrile/water 70/30. The limit of quantification (LOQ) was 0.10 µg/L which was the lowest concentration of the calibration curves (linear regression, $R^2 > 0.99$). The data were elaborated using Chromeleon™ 6.8 software.

The by-products resulting from the degradation of LEV were extracted using ethyl acetate. After extraction, the residues were dehydrated with anhydrous $Na_2SO_4$, subjected to evaporation until dryness, and then dissolved in a small volume of methanol of HPLC grade. Identification of the degradation by-products was carried out using Gas Chromatography Mass Spectrometry (GC/MS) (Agilent 7890 (Agilent, Palo Alto, CA, USA) equipped with the mass detector MSD 5977) with a Supelco® SPB-5 capillary column (30 $m\times$ 250 µm × 0.25 µm). Helium

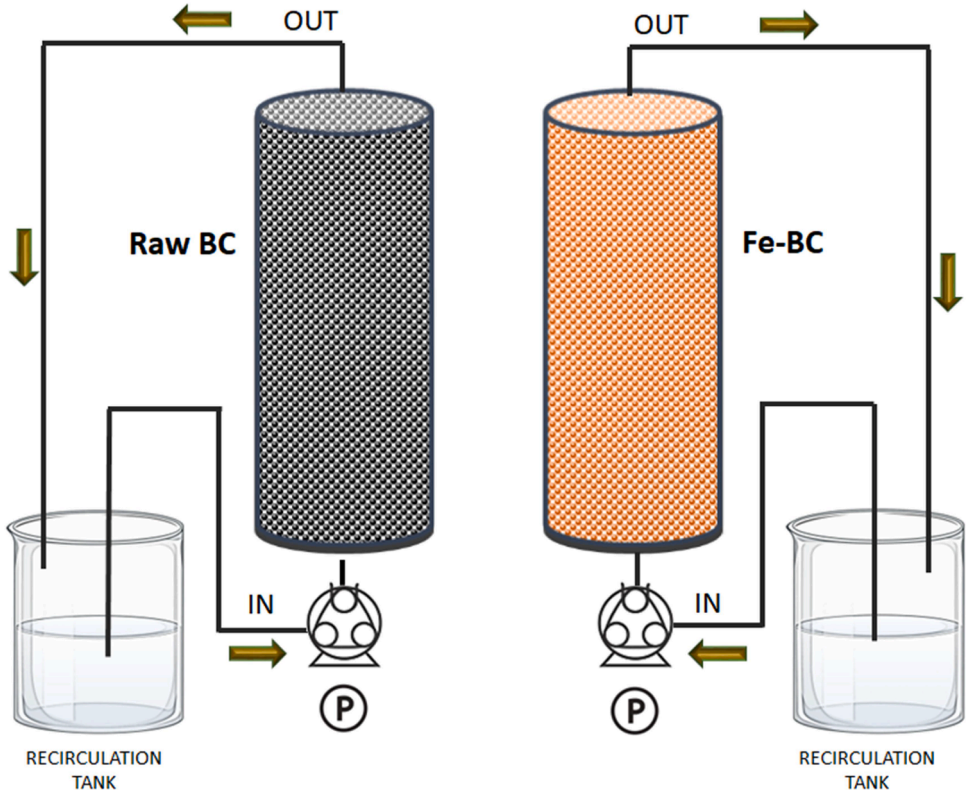


**Fig. 1.** Experimental set-up.

served as the carrier gas at a flow rate of 1.0 mL $min^{-1}$. The oven temperature profile was programmed as follows: initial equilibration at 50 °C for 5 min, followed by a temperature ramp to 300 °C at a rate of 10 °C $min^{-1}$, held for 10 min. The mass spectrometer operated in electron impact ionization mode at 70 eV, producing full-scan mass spectra at a rate of 2400 scans $min^{-1}$ within a mass range ($m/z$) of 50–400. The source and transfer line temperatures for the mass spectrometer were set at 230 and 280 °C, respectively. A mass spectral search was conducted using the National Institute for Standard Technology's (NIST) mass spectral library. By-products were identified based on their mass spectrum in conjunction with the NIST library.

### 2.6.2. Residual oxidants and iron determination

To assess residual $S_2O_8^{2-}$, spectrophotometric analysis was used, which was based on a previously described method that involved changing the iodometric titration methodology [44]. In summary, the absorption spectra of a yellow-coloured solution generated by the interaction of persulfate and iodide in the presence of sodium bicarbonate showed an absorbance at 352 nm with little interference from the reagent matrix. The calibration curve demonstrated linearity from 0 to 1 g/L.

The residual $H_2O_2$ content was evaluated using a spectrophotometric approach employing titanium(IV)oxysulfate, which forms a stable yellow complex with $H_2O_2$ and is visible at 410 nm [45]. The absorbance measurement revealed a linear relationship with standard $H_2O_2$ values ranging from 0.1 to 100 mg/L [46]. The concentration of ferrous ions in the solution, resulting from leaching, was determined using an adapted 1,10-phenanthroline methodology. In this process, ferrous iron forms a coloured complex upon reacting with 1,10-phenanthroline. The quantification of ferrous ion levels was achieved by measuring the absorbance of the formed colored complex with a UV–Vis spectrophotometer at a wavelength of 508 nm. Additionally, the concentration of ferric ions was assessed through the ferric–salicylic acid complexation method. For this measurement, 5 mL of a 100 mg/L salicylic acid solution was combined with 5 mL of a ferric solution/sample in a conical flask, thoroughly mixed, and the resulting violet-colored solution was analyzed at a 525 nm wavelength [47].

### 2.7. Kinetic study

The kinetics of $H_2O_2$, $S_2O_8^{2-}$ and LFX were mathematically described, considering the reaction scheme outlined in Table 2 for oxidation and also considering the adsorption process. The adsorption was modelled by using a pseudo-first order (PFO) kinetic, based on the results of this study and on the results obtained in previous literature works [48–51], through the following equation (Eq. 4).

$$[LFX] = [LFX]_0 e^{-kt} \quad (4)$$

The oxidation reaction scheme was developed based on scavenging tests and different hypotheses from the literature [52–55]. The scheme relies on the following assumptions:

i) The only oxidizing species considered were $^{\bullet}OH$ and $^{\bullet}OOH$ for Fe-BC/$H_2O_2$ while $SO4^{\bullet-}$ and $^{\bullet}OH$ for Fe-BC/$S_2O_8^{2-}$.
ii) The oxygen concentration is always in excess.

Then, these assumptions allowed to obtain the reaction rate expressions, for the studied species (Table 3).

The system of differential equations was solved utilizing the MATLAB 2023b function "ode23s," and the model parameters were determined through the built-in optimization routine "fmincon" [58,59]. The results of the fitting were evaluated in terms of correlation coefficient ($R^2$) and root mean square error (RMSE, Eq. 5).

$$RMSE = \sqrt{\sum_{i=1}^{n} \frac{(\hat{y}_i - y)^2}{n}} \quad (5)$$

Where:

**Table 2**
Reaction schemes considered for kinetic study.

| | Reactions | $k_i$ ($M^{-1}\,s^{-1}$) |
|---|---|---|
| | Fe-BC/$H_2O_2$ process | |
| $r_1$ | $Fe^{2+} + H_2O_2 \xrightarrow{k_1} Fe^{3+} + HO^{\cdot} + HO^-$ | 63[a] |
| $r_2$ | $Fe^{3+} + H_2O_2 \xrightarrow{k_2} Fe^{2+} + HOO^{\cdot} + H^+$ | 0.01[a] |
| $r_3$ | $Fe^{2+} + HO^{\cdot} \xrightarrow{k_3} Fe^{3+} + HO^-$ | $4.8 \times 10^8$ [a] |
| $r_4$ | $H_2O_2 + HO^{\cdot} \xrightarrow{k_4} HOO^{\cdot} + H_2O$ | $7 \times 10^7$ [b] |
| $r_5$ | $Fe^{3+} + HOO^{\bullet} \xrightarrow{k_5} Fe^{2+} + H^+ + O_2$ | $3.1 \times 10^5$ [c] |
| $r_6$ | $HO^{\cdot} + HO^{\cdot} \xrightarrow{k_6} H_2O_2$ | $4.2 \times 10^9$ [c] |
| $r_7$ | $HOO^{\cdot} + HOO^{\cdot} \xrightarrow{k_7} H_2O_2 + O_2$ | $8.3 \times 10^5$ [c] |
| $r_8$ | $HO^{\cdot} + HOO^{\cdot} \xrightarrow{k_8} H_2O + O_2$ | $1 \times 10^{10}$ [c] |
| $r_9$ | $LFX + HO^{\cdot} \xrightarrow{k_9} LFX_i$ | $k_9$[d] |
| | Fe-BC/$S_2O_8^{2-}$ process | |
| $r_{10}$ | $Fe^{2+} + S_2O_8^{2-} \xrightarrow{k_{10}} Fe^{3+} + SO_4^{\cdot-} + SO_4^{2-}$ | 15.33[a] |
| $r_{11}$ | $Fe^{2+} + SO_4^{\bullet-} \xrightarrow{k_{11}} Fe^{3+} + SO_4^{\cdot-} + SO_4^{2-}$ | $4.6 \times 10^4$ [a] |
| $r_{12}$ | $Fe^{2+} + SO_4^{\cdot-} \xrightarrow{k_{12}} Fe^{3+} + SO_4^{2-}$ | $4.6 \times 10^9$ [a] |
| $r_{13}$ | $S_2O_8^{2-} + SO_4^{\cdot-} \xrightarrow{k_{13}} S_2O_8^{\cdot-} + SO_4^{2-}$ | $6.62 \times 10^5$ [a] |
| $r_{14}$ | $SO_4^{\cdot-} \xrightarrow{k_{14}} HO^{\cdot} + HSO_4^-$ | $9.4 \times 10^3$ [a] |
| $r_{15}$ | $SO_4^{\cdot-} + SO_4^{\cdot-} \xrightarrow{k_{15}} S_2O_8^{2-}$ | $8.1 \times 10^8$ [a] |
| $r_{16}$ | $S_2O_8^{2-} + HO^{\bullet} \xrightarrow{k_{16}} HSO_4^- + SO_4^{\bullet-} + \frac{1}{2}O_2$ | $1.2 \times 10^7$ [a] |
| $r_{17}$ | $SO_4^{\cdot-} + HO^{\cdot} \xrightarrow{k_{17}} HSO_4^- + \frac{1}{2}O_2$ | $1.0 \times 10^{10}$ [a] |
| $r_{18}$ | $LFX + SO_4^{\cdot-} \xrightarrow{k_{18}} LFX_i$ | $k_{18}$[d] |
| | Adsorption process (Fe-BC) | |
| $r_{19}$ | $[LFX] = [LFX]_0 e^{-k_{19}t}$ | $k_{19}$[d] |

[a] [56].
[b] [53].
[c] [57].
[d] value calculated in this work.

$\hat{y}_i$ = predicted values
$y$ = measured values
$n$ = number of observations

## 3. Results and discussions

### 3.1. Biochar characterization

The FTIR spectra of the raw and functionalized biochar samples are shown in Fig. 2. The raw biochar (blue line) exhibits several characteristic peaks, such as the O—H stretching vibration at 3420 $cm^{-1}$, the C—H stretching vibration at 2920 $cm^{-1}$, the C = O stretching vibration at 1720 $cm^{-1}$, and the C—O stretching vibration at 1050 $cm^{-1}$. These peaks indicate the presence of various functional groups on the biochar surface, such as hydroxyl, aliphatic, carbonyl, and ether groups. These groups can affect the physicochemical properties and the reactivity of the biochar. The functionalized biochar (red line) shows a similar spectrum, but with some differences. The most noticeable difference is the appearance of a strong peak at 575 $cm^{-1}$, which can be attributed to the Fe-O stretching vibration of iron oxide. This confirms the successful loading of iron oxide onto the biochar surface. Iron oxide is a well-known catalyst and adsorbent that can enhance the performance of

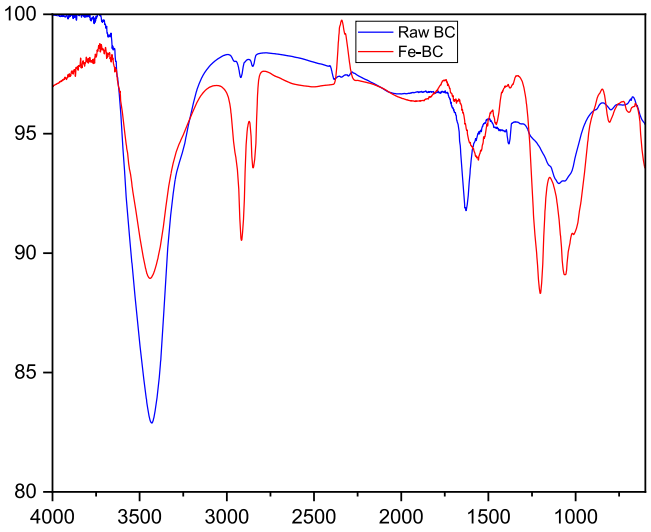


**Fig. 2.** FTIR spectrum of RBC (blue line) and Fe-BC (red line).

**Table 3**
Reaction rates for the studied species.

Reaction rate expressions
$Fe^{2+}/H_2O_2$ process

$$\frac{d[Fe^{2+}]}{dt} = -r_1 + r_2 - r_3 + r_5$$
$$\frac{d[Fe^{3+}]}{dt} = -\frac{d[Fe^{2+}]}{dt}$$
$$\frac{d[H_2O_2]}{dt} = -r_1 - r_2 - r_4 + r_6 + r_7$$
$$\frac{d[HO^{\bullet}]}{dt} = r_1 - r_3 - r_4 - r_6 - r_8 - r_9$$
$$\frac{d[HOO^{\bullet}]}{dt} = r_2 + r_4 - r_5 - r_7 - r_8$$
$$\frac{d[LFX]}{dt} = -r_9 - r_{19}$$

$Fe^{2+}/S_2O_8^{2-}$ process

$$\frac{d[Fe^{2+}]}{dt} = -r_{10} - r_{11} - r_{12}$$
$$\frac{d[Fe^{3+}]}{dt} = -\frac{d[Fe^{2+}]}{dt}$$
$$\frac{d[S_2O_8^{2-}]}{dt} = -r_{10} - r_{13} + r_{15} - r_{16}$$
$$\frac{d[SO_4^{\bullet-}]}{dt} = r_{10} + r_{11} - r_{12} - r_{13} - r_{14} - r_{15} + r_{16} - r_{17} - r_{18}$$
$$\frac{d[HO^{\bullet}]}{dt} = r_{14} - r_{16} - r_{17}$$
$$\frac{d[LFX]}{dt} = -r_{18} - r_{19}$$

the biochar in various applications, such as wastewater treatment, soil remediation, and energy production. Another difference is the increase in the intensity of the C = O peak at 1720 $cm^{-1}$, which suggests the formation of carboxylic groups on the biochar surface during the functionalization process. These groups can act as ligands for the iron oxide nanoparticles and enhance the stability of the composite. They can also increase the acidity and the cation exchange capacity of the biochar, which can affect its interactions with other substances. The functionalized biochar also shows a slight decrease in the intensity of the O—H peak at 3420 $cm^{-1}$, which indicates a reduction in the hydrophilicity of the biochar surface. This can improve the performance of the biochar in aqueous environments, as it can reduce the water uptake and the swelling of the biochar. It can also increase the thermal stability and the carbon content of the biochar, which can improve its energy efficiency and its carbon sequestration potential.

The XRD patterns of the raw and functionalized biochar samples are shown in Fig. 3. The raw biochar (black pattern) exhibits a broad peak around 23°, which corresponds to the (002) plane of graphite. This peak indicates the presence of crystalline carbon structures in the biochar, which are formed during the pyrolysis process. The crystallinity of the biochar can affect its porosity, surface area, and electrical conductivity, which are important parameters for its applications. The functionalized biochar (orange pattern) shows a similar peak, but also displays several sharp peaks at 24.1°, 33.2°, 35.6°, 40.9°, 49.5°, 54.1°, 57.6°, and 62.5°, which can be assigned to the (012), (104), (110), (113), (024), (116), (018), and (214) planes of hematite ($Fe_2O_3$), respectively. These peaks confirm the successful loading of iron oxide nanoparticles onto the biochar surface during the functionalization process. Iron oxide is a well-known catalyst and adsorbent that can enhance the performance of the biochar in various applications, such as wastewater treatment, soil remediation, and energy production. The XRD patterns also show the effect of the functionalization process on the crystallinity of the biochar. The functionalized biochar has a higher intensity of the graphite peak than the raw biochar, which suggests an increase in the crystallinity of the biochar. This can be explained by the removal of some amorphous carbon structures and the rearrangement of some carbon atoms during the functionalization process. The increase in the crystallinity of the biochar can improve its thermal stability and its carbon content, which can improve its energy efficiency and its carbon sequestration potential.

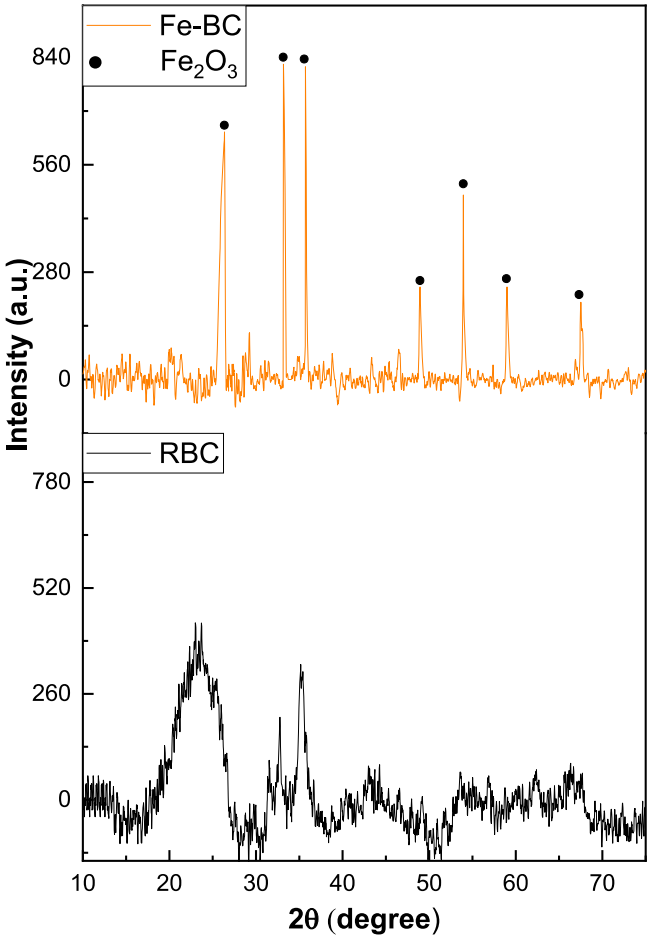


**Fig. 3.** X-ray diffractogram of RBC (black line) and Fe-BC (orange line). The black dots are associated with $Fe_2O_3$ crystalline peaks.

### 3.2. Factor analysis of mixed data

FAMD was utilized to understand the relationships among various variables such as pH, oxidant dose, oxidant type, treatment time, biochar type, and the resulting LFX concentration. The first two principal factors in the FAMD explained approximately 70 % of the variance within the data. A clear separation of sample groups was evident along the second dimension. The biplot (Fig. 4), which combines both the variables and observations, highlighted a strong correlation between treatment time, oxidant dose, and the response variable, particularly noticeable along the first dimension. In contrast, the second dimension showcased distinct correlations between pH levels, the type of oxidant, and the type of biochar used.

Specifically, experiments with RBC displayed a marked variability in response along the second dimension, indicating the significance of pH and oxidant type in these trials. RBC and Fe-BC formed distinct clusters on this axis, with RBC data points tending towards the positive quadrant. Furthermore, the proximity of variable vectors in the biplot suggested a strong correlation among them. The results from RBC trials exhibited greater variability with different oxidants, while Fe-BC trials demonstrated less variance and generally higher efficiencies across both oxidants. Along the first dimension, there was a notable correlation between treatment time, oxidant dose, and LFX concentration, particularly in trials involving Fe-BC, where data points spread more into the positive abscissa and negative ordinate quadrant. This indicates that the interaction between treatment time and oxidant dose was crucial in experiments with Fe-BC.

### 3.3. Experimental design and process optimization

After FAMD, the removal of LFX by fixed-bed Fenton process with BC or Fe-BC as catalyst and $H_2O_2$ and $S_2O_8^{2-}$ as oxidant agents was optimized by RSM analysis to evaluate its applicability in CECs removal from WW. The response values (final LFX concentration) were transformed into natural-log values to better show the differences between them and to normalize the distribution. The fitted model was cubic and the coefficient of determination of the model was found to be $R^2$=0.9329. The disparities between the predicted and adjusted $R^2$ values were within the margin of 0.2. Fig. 5 shows the 3D response surfaces for each condition (namely RBC/$H_2O_2$, Fe-BC/$H_2O_2$, RBC/$S_2O_8^{2-}$ and Fe-BC/$S_2O_8^{2-}$). All the surface plots are shown at the middle point for pH factor (i.e., 5.8).

Fig. 5a shows the 3D response plot for LFX removal with RBC/$H_2O_2$. When the $H_2O_2$ concentration was zero (thus assessing only the adsorption effect), it was observed that the adsorption capacity was time dependent. Specifically, from the minimum treatment time (2 min) to 30 min, there was a removal increase of LFX by 2.7-ln units. After one hour of treatment, the removal increment was 3.03-ln units. With the increase in oxidant concentration, an enhancement in removal was observed due to the oxidation effect. Specifically, when the oxidant dose was 1.6 mM, an increase in removal of 5.52-ln units was observed after approximately 20 min, while at 60 min, there was an increase of 5.76-ln units. As the oxidant dose increased, no substantial improvement in LFX removal was observed.

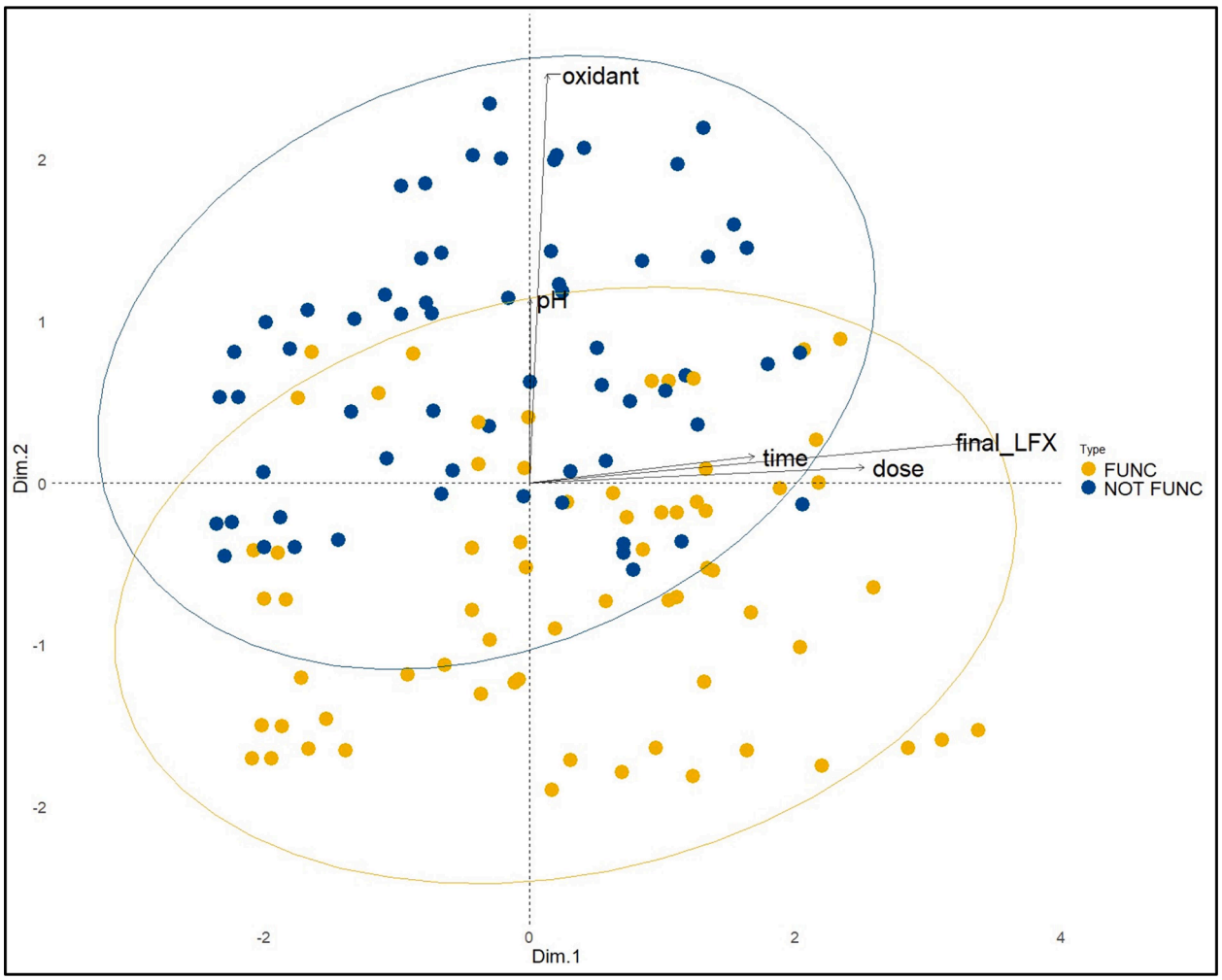


**Fig. 4.** biplot showing the first two principal dimensions obtained from FAMD.

When RBC was replaced with Fe-BC in the process assisted by $H_2O_2$ (Fe-BC/$H_2O_2$, Fig. 5b), an increase in LFX removal was observed, starting from the adsorption process alone (i.e., $H_2O_2$ concentration at zero). Specifically, after 2 min, there was a substantial increase in removal of 3.2-ln units. At 30 and 60 min, a slight additional increase in removal of approximately 0.1-ln units was observed. The improvement observed in adsorption is attributed to the larger surface area exhibited by Fe-BC compared to RBC. When $H_2O_2$ concentration was 1.6 mM, a substantial increase in LFX removal was observed. Indeed, at 2 min, there was an increase of 1.73-ln units compared to the same condition in the absence of iron, while at 30 min, the increment was 2.12-ln units. At 60 min, the increase remained around 2.1-ln units compared to RBC. When $H_2O_2$ concentration was 2.5 mM, the increase in LFX removal was about 0.5-ln units for each treatment time. Therefore, it can be affirmed that the contribution of heterogeneous Fenton was evident, as also depicted graphically in Fig. 5a and b. When RBC and Fe-BC were tested with $S_2O_8^{2-}$, a general decrease in removal efficiencies was observed. Specifically, in the RBC/$S_2O_8^{2-}$ process (Fig. 5c), at low treatment times, the concentration maximizing LFX removal was found to be 1.6 mM. Increasing the oxidant concentration resulted in a deterioration of removal efficiencies. From the comparison between $H_2O_2$ and $S_2O_8^{2-}$, it was observed that at a treatment time of 2 min, $H_2O_2$ outperforms (3.2-ln units vs. 2.6-ln units). However, increasing the oxidant dose resulted in a decrease in LFX removal. At an oxidant concentration of 1.6 mM and a treatment time of 30 min, an increase in LFX removal by 2.35-ln units was observed. At 60 min, the increment was 0.1-ln units compared to the 30-minute time point. In the presence of Fe-BC, in the Fe-BC/$S_2O_8^{2-}$ process, the response surface trend closely resembles the RBC/$S_2O_8^{2-}$ process. In this case as well, the highest LFX removal was achieved at an $S_2O_8^{2-}$ concentration of 1.6 mM. Concerning treatment times, a reduction in LFX of 4.31-ln units was observed already at 30 min, with no significant improvements at 60 min. At 60 min, the increment in LFX removal in the presence of Fe-BC was approximately 1.45-ln units compared to the process employing RBC. Comparing Fe-BC/$H_2O_2$ and Fe-BC/$S_2O_8^{2-}$ processes, it is evident that the Fe-BC/$H_2O_2$ process allows for the removal of an additional 5.5-ln units of LFX.

In summary:

- The Fe-BC acted as a better adsorptive material respect to RBC.
- Fe-BC increased the LFX removal, compared to RBC, for the same amount of oxidant and the same time of the reaction.
- Fe-BC showed also catalytical behaviour for the heterogeneous Fenton reaction, improving the oxidation of LFX from water.
- $H_2O_2$ increased the percentage of LFX removal compared to $S_2O_8^{2-}$, for the same type of biochar and the same time of the reaction.

The results obtained at each pH investigated are showed in Table SM1. Results showed that the pH had a high influence on LFX removal, with different effects depending on the oxidant used. Specifically, Fe-BC/$H_2O_2$ led to better results at circumneutral pH values while, on the contrary, $S_2O_8^{2-}$ worked better at more acidic conditions. After the RSM analysis, the best conditions resulted to be:

1) Adsorption: Fe-BC at pH 5.8

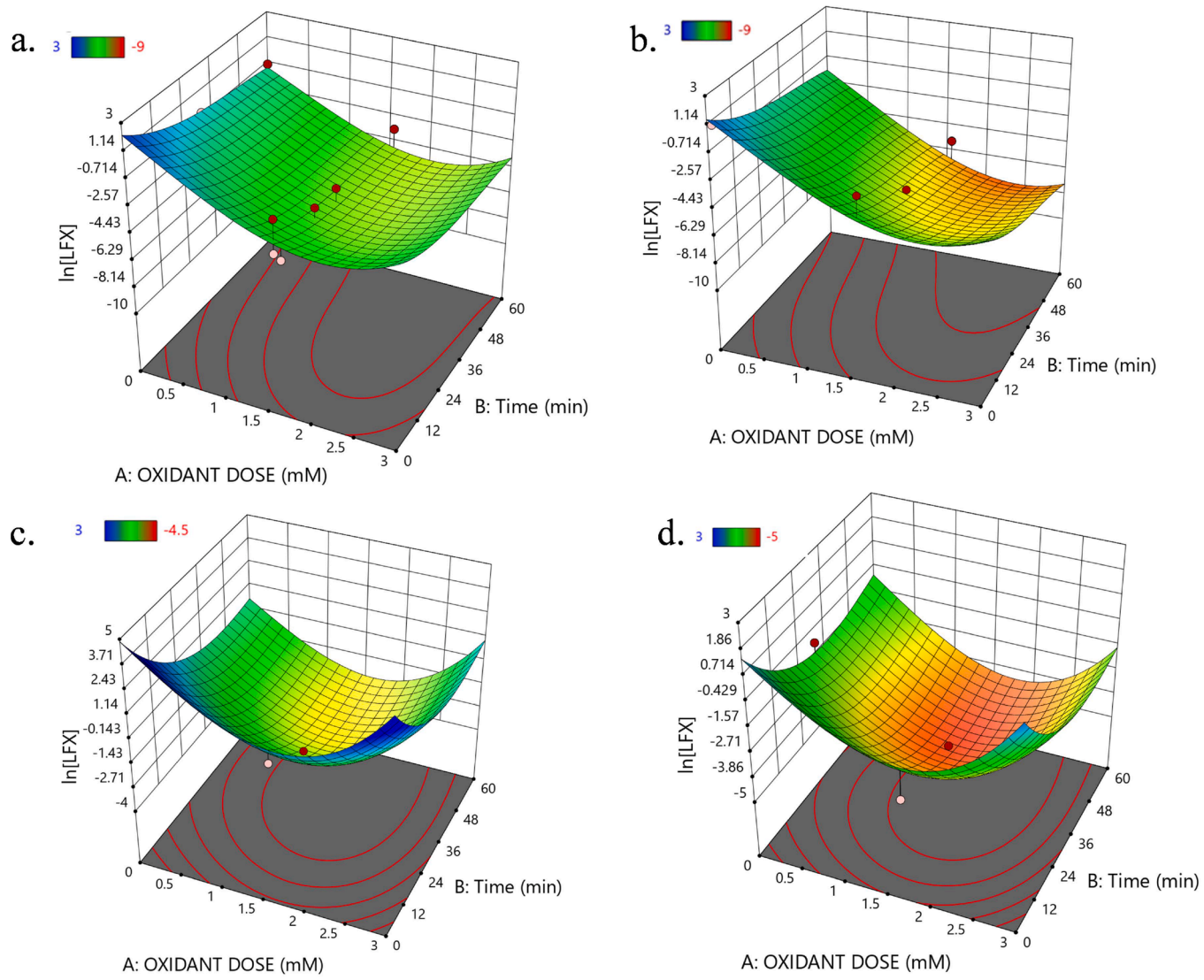


**Fig. 5.** Response plots for LFX removal with RBC/$H_2O_2$ (a), Fe-BC/$H_2O_2$ (b) RBC/$S_2O_8^{2-}$ (c) and Fe-BC/$S_2O_8^{2-}$.

2) Oxidation with $H_2O_2$: Fe-BC at pH 7.5 and 2.5 mM of $H_2O_2$
3) Oxidation with $S_2O_8^{2-}$: Fe-BC at pH 2.8 and 1.6 mM of $S_2O_8^{2-}$

These results agree with other literature works. Several studies have been conducted on the degradation of antibiotics by carbon-based-functionalized materials and $S_2O_8^{2-}$ or $H_2O_2$ as oxidant. Yao et al. 2021 [60] studied the adsorption of LFX onto biochar/$MgFe_2O_4$ composite and found a maximum LFX adsorption at pH around 5 whit a decrease at pH $\leq$ 3 and pH $\geq$ 9. LFX can exist in cationic ($LFX^+$), anionic ($LFX^-$) or molecular ($LFX^0$) form in aqueous solution ($pK_{a1}$= 6.02 and $pK_{a2}$=8.15). So, when pH $\leq$ 6.02 or pH $\geq$ 8.15, the adsorption of LFX can be inhibited by electrostatic repulsion because the surface of iron-functionalized-biochar is charged [61].

Wang et al. (2023) [62] studied the degradation of tetracycline from aqueous solution by employing a Fe-BC obtained in a similar way compared to the present work in combination with $S_2O_8^{2-}$. They also studied the effect of pH on the removal efficiency and found that at a pH of 3 the removal efficiency was the highest. A possible reason can be ascribed to the higher amount of iron released in the solution at acidic pH which favours the activation of $S_2O_8^{2-}$.

Surprisingly, in the case of $H_2O_2$, the optimal condition suggests a circumneutral pH. Again, this may be due to the increased adsorption of $LEV^0$ at 6.02 $\leq$ pH $\leq$ 8.15, which favours its degradation. Furthermore, in many cases, heterogeneous Fenton systems give the best results at a wider pH range and, in many cases, at a circumneutral pH [27,63–65]. In literature emerges that heterogeneous Fenton process allow to an increase in the range of pH at which the generation of $^{\bullet}OH$ radicals and the organic pollutants degradation occur [66,67]. Other authors showed the extension of the pH range for different heterogenous Fenton processes. In particular, Wang et al. observed same degradations for methylene blue with heterogeneous Fenton process employing carbon@Fe composite and $H_2O_2$ as oxidant agent at pH: 3 and pH: 7 [68]. Yao and co-workers found that Fe@activated carbon composite exhibited remarkable catalytic activity at neutral or basic pH values [63]. This comprehensive analysis underscores the nuanced interplay between pH levels and the efficacy of heterogeneous Fenton processes, highlighting the importance of optimizing environmental conditions to enhance pollutant degradation. The contrasting optimal pH conditions for $S_2O_8^{2-}$ and $H_2O_2$ further emphasize the necessity of a tailored approach in the application of Fenton processes, catering specifically to the chemical nature of the pollutant and the chosen oxidant.

### 3.4. Kinetics of optimized processes

According to FAMD and RSM analysis, the optimal conditions for effectively removing LFX from water with each investigated process are:

i) Fe-BC, pH: 5.8 (adsorption)
ii) Fe-BC/$S_2O_8^{2-}$ (1.6 mM), pH: 2.8 (oxidation)
iii) Fe-BC/$H_2O_2$ (2.5 mM), pH: 7.5 (oxidation)

The same conditions were used also substituting Fe-BC with RBC for comparison and to evaluate the catalytic effect of the functionalized material. Fig. 6a and Fig. 6b show the kinetics for optimized processes and the final LFX concentration reached by each process, respectively.

When RBC and Fe-BC were used without the oxidants (i.e., adsorption processes), the maximum LFX removal was obtained by the Fe-BC, reaching a final concentration of about 335 μg/L in 60 min at pH of 5.8. The RBC, instead, at the same conditions, allowed to reach a final value of about 530 μg/L. The maximum adsorption capacity ($Q_{max}$) for Fe-BC was 272 μg/g.

The oxidative processes enabled the attainment of excellent removal of LFX. Fe-BC/$S_2O_8^{2-}$ process allowed for a removal of LFX of approximately 5-ln units (final [LFX]= 2.8 μg/L). When the RBC was used in combination with $S_2O_8^{2-}$, the removal efficiency decreased of about 1-ln unit compared to Fe-BC/$S_2O_8^{2-}$, led to a final LFX concentration of 8.9 μg/L. Compared to RBC/$S_2O_8^{2-}$ process, the two kinetics are very similar but in Fe-BC/$S_2O_8^{2-}$ one the effect of the catalyst loading (Fe) is evident.

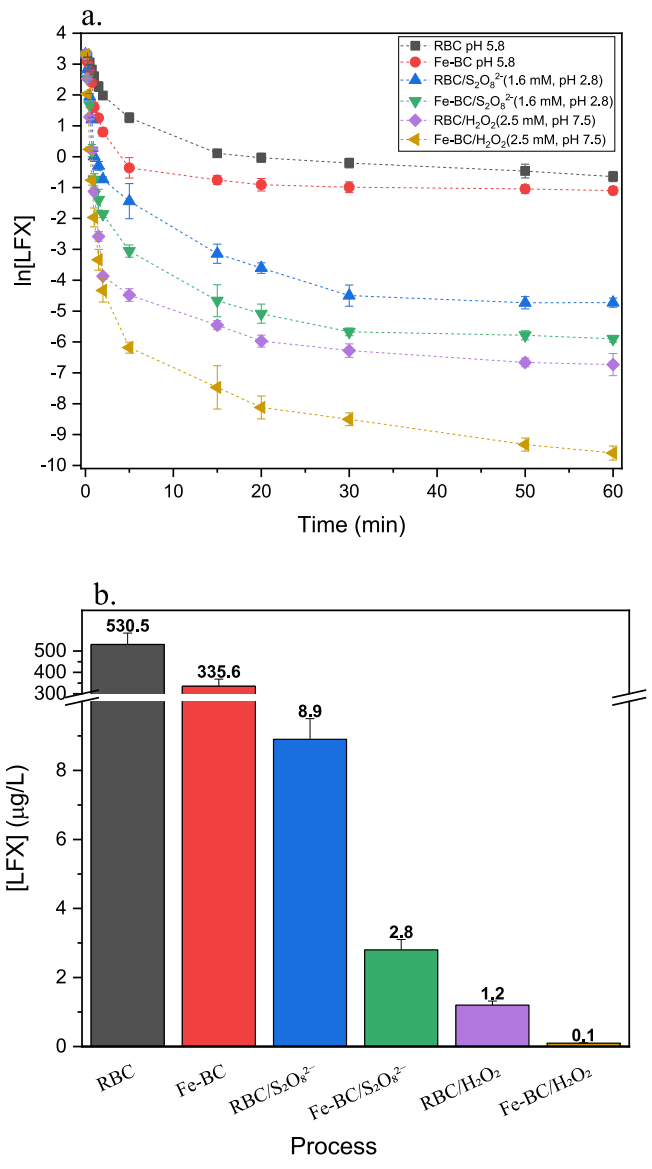


**Fig. 6.** kinetics for optimized processes (a) and final LFX concentration reached by each process (b).

When Fe-BC/$S_2O_8^{2-}$ process was replaced by Fe-BC/$H_2O_2$, higher LFX removals (up to 4.5-ln units) were obtained. Fe-BC/$H_2O_2$ process allowed for a removal of LFX of approximately twice as higher as Fe-BC/$S_2O_8^{2-}$ one with about 9.5-ln units of removal (final [LFX]= 0.1 μg /L). When the RBC/$H_2O_2$ was tested, the removal efficiency was about 1-ln unit higher compared to Fe-BC/$S_2O_8^{2-}$, led to a final LFX concentration of 1.2 μg/L. Compared to RBC/$H_2O_2$ process, the kinetics of Fe-BC/$H_2O_2$ is much faster, and the effect of the catalyst loading (Fe) is more evident. Comparing the results among themselves, it is evident that the adsorption effect with Fe-BC increases the antibiotic removal capacity by approximately 37 % compared to RBC alone. When the oxidant is used, the oxidative process generally leads to additional removals exceeding 99 % compared to adsorption alone. Comparing the process between the two oxidants, it is found that with Fe-BC/$H_2O_2$, there are percentage removal increases 92 % higher than the RBC/$H_2O_2$ process. In the case of $S_2O_8^{2-}$, the percentage increase is approximately 69 % with Fe-BC. Furthermore, from the comparison between the two processes using Fe-BC, it was observed that with $H_2O_2$, there is a 96 % increase in the percentage removal of LFX compared to the $S_2O_8^{2-}$ process.

To better understand the mechanisms involved in the LFX oxidation by Fe-BC/$S_2O_8^{2-}$ process, the degradation byproducts were detected through GC/MS analysis and four degradation pathways were proposed (Fig. 7. Mass spectra of the degradation products are available in Figure SM1):

Within these pathways, we delineate four primary oxidative transformation mechanisms, characterized by their specificity towards particular molecular moieties within LFX:

1. Targeted Decarboxylation: The carboxylic acid moiety of LFX is particularly prone to oxidative attack, leading to the formation of an initial intermediate, designated as P1 (*m/z*: 317.9). This initial reaction underscores the vulnerability of the carboxyl group to electron abstraction under oxidative stress. P1 is subject to further oxidative stress, culminating in the ring-opening and formation of P2 (*m/z*: 291.1). This step signifies a pivotal transformation, indicative of a radical chain mechanism.
2. Oxidative Ring Opening and Radical Propagation: Subsequent to decarboxylation, In parallel, direct interaction of LFX with •OH and SO4•− radicals propels the formation of P3 (*m/z*: 335.1), which is then transformed into P4 (*m/z*: 234.1) through a combination of decarboxylation and depiperazinylation—a process hinting at a multistep radical substitution followed by ring cleavage.
3. Direct Decarboxylation/Depiperazinylation: This delineates a concurrent pathway where LFX is directly subjected to decarboxylation and depiperazinylation, leading to the immediate formation of P4. This route underscores the potential for simultaneous multiple bond disruptions within the LFX molecule.
4. Sequential Demethylation/Defluorination: Specific methylation and carbon-fluorine bonds within LFX are susceptible to ROS attack, facilitating a sequence of demethylation and defluorination reactions. These transformations yield P5 (*m/z*: 281.1), indicative of a complex radical-mediated defunctionalisation.

Collectively, these intermediates undergo further oxidative degradation (P2 - depiperazinylation, P4 – 5-methyl-3,4-dihydro-2H-1,4-oxazine removal, P5 – depiperazinylation/5-methyl-3,4-dihydro-2H-1,4-oxazine removal), converging to form P6 (*m/z*: 191.1), which is subsequently reduced to smaller organic compounds (P7, P8, P9). The formation of 1-methylpyrrolidin-2-one (P7) suggests a cyclization reaction followed by a methyl group retention, indicative of the preservation of the pyrrolidine ring from the LFX structure, which has undergone significant deconstruction. This transformation is indicative of a rearrangement process, potentially through a radical-mediated pathway. The emergence of N,N-diethylformamide (P8) denotes a significant N—C bond cleavage and substitution reaction, implying that the LFX molecule's piperazine ring or other nitrogen-containing moieties

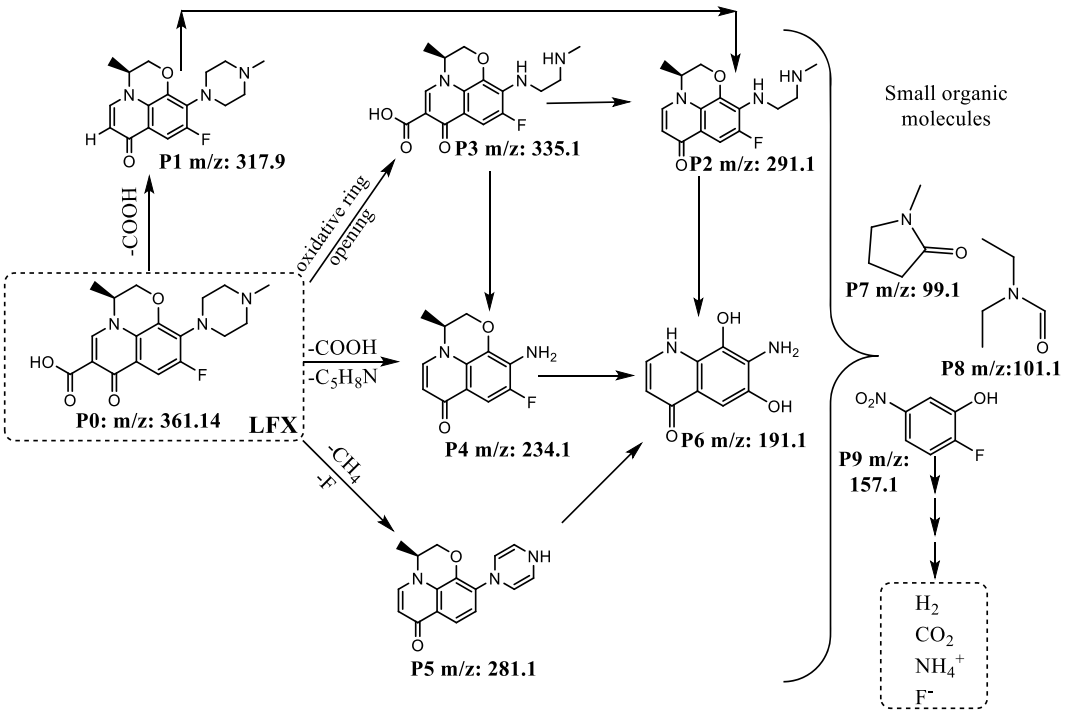


**Fig. 7.** Proposed degradation pathway for Fe-BC/$S_2O_8^{2-}$ process.

undergo dealkylation. The presence of diethylformamide is particularly revealing of the possible introduction of an ethyl group during the transformation process, likely through a transamination reaction involving the exchange of amino or amido groups. The detection of 2-fluoro-5-nitrophenol (P9) is indicative of an electrophilic aromatic substitution, where the nitro group has been introduced into the aromatic ring. The presence of both fluorine and nitro groups in P9 suggests that specific regions of the LFX molecular structure remain somewhat intact throughout the degradation process, retaining the capacity for further substitution reactions. The fluorine atom's retention also speaks to the resistance of C-F bonds to complete defluorination, while the nitration of the ring is likely a result of oxidative stress, perhaps via the interaction with nitrate radicals or other nitrogen oxides present in the reaction milieu. This culminates in the complete mineralization of the

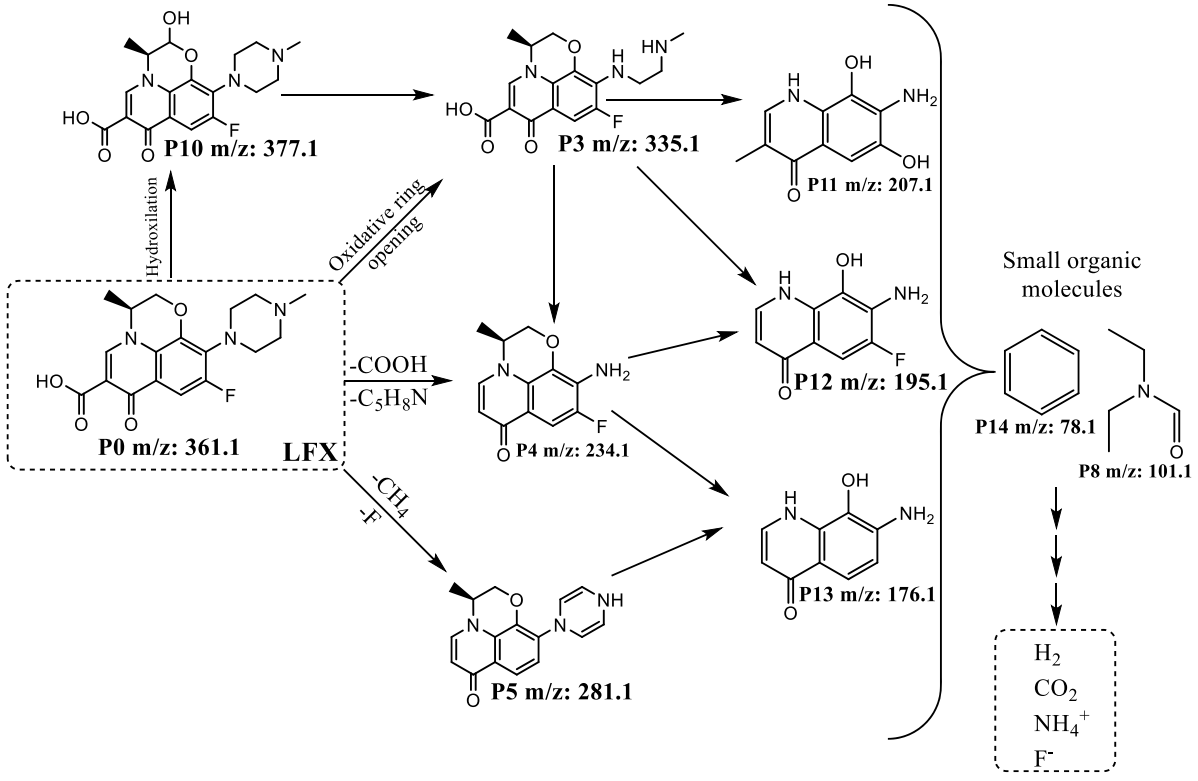


**Fig. 8.** Proposed degradation pathway for Fe-BC/$H_2O_2$ process.

molecule, reflecting a comprehensive breakdown of the complex LFX structure into its constituent inorganic atoms. These results are in agreement with other literature works in which $S_2O_8^{2-}$ supported Fenton processes were tested for LFX degradation from aqueous solutions [69, 70].

In the case of Fe-BC/$H_2O_2$, four degradation pathways were proposed (Fig 8, mass spectra at different times are available in Figure SM2).

The four pathways proposed for Fe-BC/$H_2O_2$ process were very similar to that proposed for Fe-BC/$S_2O_8^{2-}$ one but the decarboxylation is replaced by hydroxylation.

Hydroxylation, likely mediated by the highly reactive HO• radicals generated in the Fenton reaction, typically introduces hydroxyl groups to organic substrates, increasing their solubility and reactivity. The production of P10 with a molecular weight of 377.1 as a result of hydroxylation suggests the addition of one hydroxyl groups to the LFX molecule, which can drastically change the subsequent degradation behaviour of the molecule. P10 undergo an oxidative ring opening/dehydroxilation to form P3 which can undergo two different chain reactions to form P11(*m/z*: 207.1) and P12 (*m/z*: 195.1):

- of decarboxylation/depiperazinylation to form P4 and then P4 undergo a 5-methyl-3,4-dihydro-2H-1,4-oxazine removal to form P12.
- decarboxylation/depiperazinylation/5-methyl-3,4-dihydro-2H-1,4-oxazine removal.
- decarboxylation/depiperazinylation/5-methyl-3,4-dihydro-2H-1,4-oxazine removal and defluorination to form P11.

On the other hand, P4 can undergo two different pathways to led to the formation of both P12 and P13 (*m/z*: 176.1):

- the 5-methyl-3,4-dihydro-2H-1,4-oxazine removal promotes the formation of P12.
- the chain reaction defluorination/5-methyl-3,4-dihydro-2H-1,4-oxazine removal promotes the formation of P13.

P5, through the direct depiperazinylation and 5-methyl-3,4-dihydro-2H-1,4-oxazine removal, could led to the formation of P13 intermediate.

In this case also benzene (P14 *m/z*: 78.1) was detected as smaller byproduct. The detection of benzene is particularly noteworthy, as it suggests the complete deconstruction of the complex LFX molecule down to a simple aromatic hydrocarbon. This finding is intriguing, as benzene is a relatively stable compound and its formation could imply the occurrence of extensive ring-opening reactions followed by a rearrangement to reform the aromatic system, which is typical in the degradation of complex aromatic compounds. The presence of N,N-diethylformamide (P8) across different degradation systems further supports the notion of a common intermediate or mechanistic pathway, where amide and nitrogen functionalities are preserved longer in the degradation sequence before eventually breaking down. These results agree with other works in which different $H_2O_2$ supported Fenton processes were tested for LFX oxidative degradation [4,71–73]. The presence of HO• radicals in the system suggests a highly oxidative environment, favoring hydroxylation over decarboxylation and potentially leading to a more diverse array of intermediate products. The formation of smaller byproducts, such as benzene, underscores the efficiency of the Fe-BC/H2O2 system in breaking down complex organic molecules to their simplest forms, which has significant implications for the treatment of LFX-contaminated water.

### 3.5. Identification of predominant radical species

Radical inhibition experiments were carried out to discern the primary radical oxidant ($SO_4^{\bullet-}$ vs. $^{\bullet}OH$) by investigating variations in radical reactivity towards two distinct alcohol additives, namely ethanol (EtOH) and tert-butyl alcohol (TBA), as detailed in prior research [74]. The reaction rate of $SO_4^{\bullet-}$ with TBA was notably slower (4–9.1 $\times 10^5\ M^{-1}\ s^{-1}$) compared to its reaction with EtOH (1.6–7.7 $\times 10^8\ M^{-1}\ s^{-1}$). On the other hand, $^{\bullet}OH$ exhibited rapid reactivity with both EtOH and TBA. Consequently, EtOH proved to be an effective quencher for both $SO_4^{\bullet-}$ and $^{\bullet}OH$, while TBA effectively quenched $^{\bullet}OH$ but not $SO_4^{\bullet-}$ [21,74]. Specifically, scavenging tests were executed to assess the degradation of LFX in both processes (Fe-BC/$H_2O_2$ and Fe-BC/$S_2O_8^{2-}$), aiming to prevent interference from EtOH and TBA in COD measurements. Two concentrations of each alcohol, namely 2.5 mM and 50 mM, were employed in the Fe-BC/$H_2O_2$ experiments while 1.6 mM and 30 mM were employed in Fe-BC/$S_2O_8^{2-}$ experiments (Fig. 9a and Fig. 9b).

Fig. 9 illustrates the rate of LFX degradation in the presence of quenching reagents. The addition of 2.5/1.6 mM and 50/30 mM of EtOH significantly inhibited catalytic activity for LFX degradation in both processes. However, the addition of TBA had a substantial impact only on the Fe-BC/$H_2O_2$ process. This outcome suggests that the predominant radical formed in the Fe-BC/$S_2O_8^{2-}$ process is $SO_4^{\bullet-}$. While hydroxyl radicals might also be present in the Fe-BC/$S_2O_8^{2-}$ process, their contribution is minimal compared to sulphate radicals.

### 3.6. Kinetic modelling

As can be seen from Fig. 10, the kinetic model developed in this work well reproduced the decrease of LFX and the oxidants consumption in all the conditions. The parameters obtained for each species in each process are presented in Table 4.

As can be noted, $k_9$ and $k_{18}$, the kinetic constants associated with the reactions of LFX with $HO^{\bullet}$ and $SO_4^{\bullet-}$ respectively, are about 2 time higher than $k_{19}$, the kinetic constant for PFO adsorption process, in both oxidation processes, confirming that the oxidation process is more rapid than the adsorption one. Also, it is very interesting to note that, when performed alone, the adsorption process kinetic constant ($k_{19}$) associated at Fe-BC, is about 4 and 2.5 times lower than the $k_{19}$ of Fe-BC/$H_2O_2$ and Fe-BC/$S_2O_8^{2-}$ processes respectively. The higher adsorption rate is associated with the more rapid oxidation of LFX and the higher adsorption of by-products (which contains several charged functional groups as can be seen in Fig. 7 and Fig. 8) on the surface of Fe-BC. The oxidant consumption was very high for both $S_2O_8^{2-}$ and $H_2O_2$, with residual concentrations $< 0.1$ mg/L. The high $H_2O_2$ activation rate at neutral pH can be justified by the fact that the biochar itself is a good $H_2O_2$ activator for the generation of hydroxyl radicals [75] and because the heterogeneous catalysts expand the pH range for Fenton processes [66].

### 3.7. Iron leaching

In the context of this research, the operational effectiveness of heterogeneous catalysis was analyzed with a focus on iron ion leachability and the intrinsic catalytic properties of the catalyst's solid surface. Our investigation delves into the dynamics of Fe-BC in a fixed-bed configuration for the treatment of water contaminated with LFX, utilizing $H_2O_2$ and $S_2O_8^{2-}$ as oxidizing agents. Observational data from our experimental setup indicated that the leached iron ion concentration within the aqueous phase remained consistently below 1 mg/L (Fig. 11).

The results obtained allowed to confirm the occurrence of heterogenous oxidation. In fact, in the present work, the $H_2O_2$/leached-$Fe^{2+}$ ratio was 274 and $H_2O_2$/leached-$Fe^{2+}$ one was 156. These ratios are very low and, normally, higher $H_2O_2$/iron ratios (from 1/1 to 50/1), with a higher iron concentration, are required to effectively perform conventional homogeneous Fenton process for the degradation of lesser antibiotic concentration [76–78]. The significance of these findings is twofold. Firstly, it directly addresses the concerns related to the depletion of active catalytic sites due to iron leaching, a common caveat

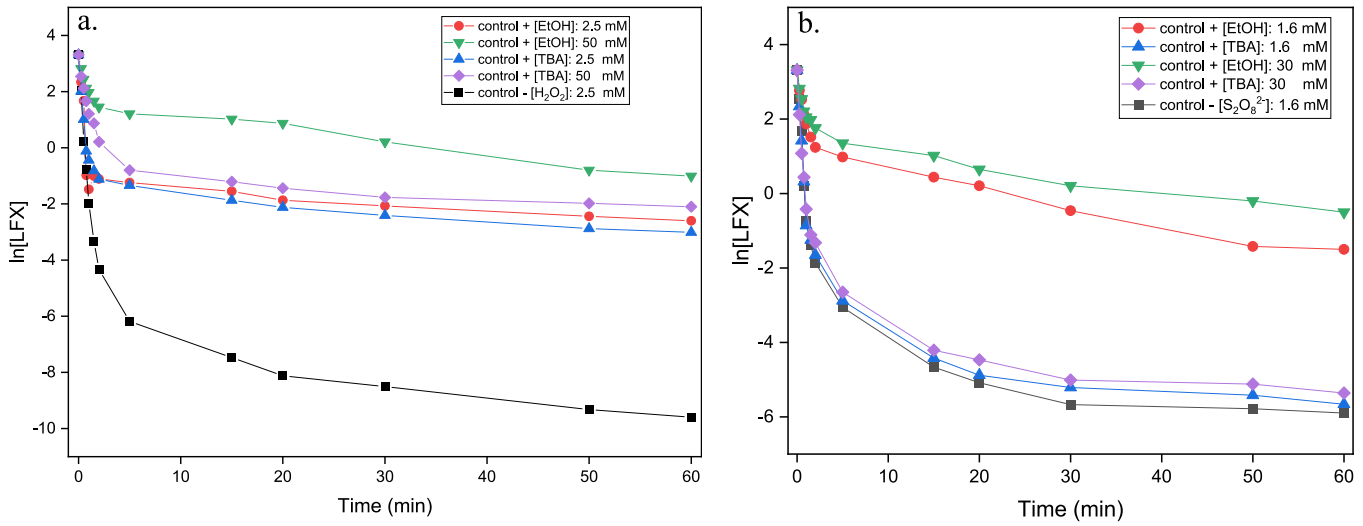


**Fig. 9.** Rates of LFX degradation in the presence of quenching agents for Fe-BC/$H_2O_2$ (a) and Fe-BC/$S_2O_8^{2-}$ (b) processes.

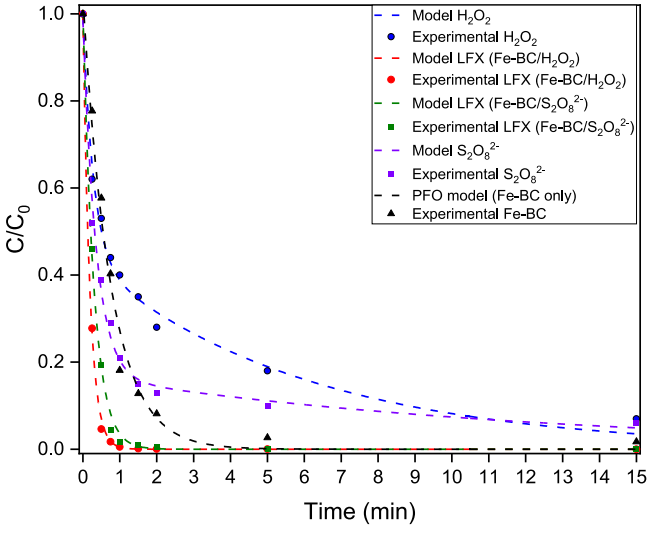


**Fig. 10.** Experimental and model results for $H_2O_2$, $S_2O_8^{2-}$ and LFX, in relative concentrations. $[H_2O_2]_0 = 2.5$ mM, $[S_2O_8^{2-}]_0 = 1.6$ mM.

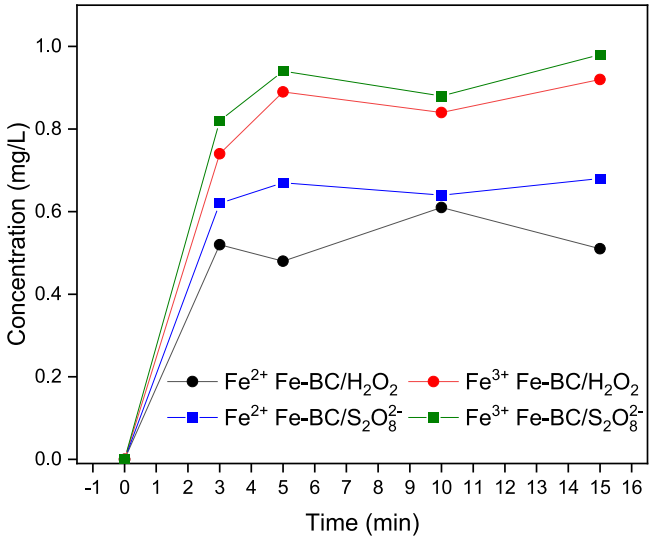


**Fig. 11.** Leaching of ferrous and ferric ions from heterogeneous Fe-BC catalysts.

**Table 4**
Model parameters obtained for each species in each process.

| Process | Species | $R^2$ | RMSE (%) | SSE (%) | $\lvert k_9 \rvert$ ($M^{-1}s^{-1}$) | $\lvert k_{18} \rvert$ ($M^{-1}s^{-1}$) | $\lvert k_{19} \rvert$ ($M^{-1}s^{-1}$) |
|---|---|---|---|---|---|---|---|
| (Fe-BC/$H_2O_2$) | LFX | 0.999 | 1 | 0.074 | 11 | – | 5.34 |
| | $H_2O_2$ | 0.987 | 3.1 | 0.048 | | | |
| (Fe-BC/$S_2O_8^{2-}$) | LFX | 0.997 | 1.8 | 0.023 | – | 8 | 3.34 |
| | $S_2O_8^{2-}$ | 0.988 | 3 | 0.052 | | | |
| (Fe-BC) | LFX | 0.983 | 4.7 | 1.5 | – | – | 1.34 |

associated with long-term utilization of heterogeneous catalysts in Fenton-like reactions. Secondly, it offers a possible solution to the environmental challenge posed by the generation of sludge, a byproduct of the iron leaching process. In homogeneous Fenton processes, the dissolution of iron ions can lead to the formation of a substantial volume of insoluble iron hydroxide complexes, exacerbating secondary pollution issues. Our results indicate that the Fe-BC catalyst, through its low iron leaching profile, significantly minimizes sludge production, which was not measurable, thereby alleviating the environmental impact. These results agree with other literature works. In particular, Rubeena and co-workers found very similar results by employing iron-modified BC for the removal of acid red 1 dye [34]. At the same way, Maćerak et al., found good structural stability of zero-valent-iron-BC catalyst, showing the minimal iron leaching from the carbonaceous matrix during wastewater treatment process [79].

## 4. Conclusions

In this work, the utilization of iron-modified biochar as a catalyst, in combination with $H_2O_2$ and $S_2O_8^{2-}$, was tested in the degradation and mineralization of LFX from water with a fixed-bed configuration, demonstrating promising potential. The results demonstrate the significant impact of various factors such as pH, oxidant type, treatment time, and biochar type on the degradation process. The use of FAMD and RSM provides a robust analytical framework for navigating the complexities of experimental data and optimizing the removal of LFX. Fe-BC significantly outperforms RBC in the removal of LFX from aqueous solutions. The Fe-BC showcases superior adsorptive characteristics, likely due to its larger surface area, and exhibits a catalytic prowess in the

heterogeneous Fenton reaction, which enhances the oxidation of LFX. Empirical evidence from the study indicates a notable increment in LFX removal of 3.2-ln units within the initial 2 min of treatment using Fe-BC with $H_2O_2$, and a consistent removal efficiency with an increase of approximately 2.1-ln units observed at the 60-minute mark. This is in stark contrast to the RBC/$S_2O_8^{2-}$ process, which peaked at a 1.6 mM oxidant concentration, beyond which a decline in removal efficiency was noted. Comparatively, Fe-BC in conjunction with $H_2O_2$ achieved an additional 5.5-ln unit removal of LFX, underscoring the efficacy of $H_2O_2$ over $S_2O_8^{2-}$ under identical conditions. Furthermore, our data suggest that the pH plays a pivotal role in the removal process, with Fe-BC/$H_2O_2$ showing optimal results at circumneutral pH, while $S_2O_8^{2-}$ is more effective in acidic environments. Based on the results obtained, the optimized conditions resulted to be: i) pH: 5.8 for adsorption process (Fe-BC only); ii) pH: 2.8 and $S_2O_8^{2-}$: 1.6 mM for Fe-BC/$S_2O_8^{2-}$ process and iii) pH: 7.5 and $H_2O_2$: 2.5 mM for Fe-BC/$H_2O_2$ process. Under optimal conditions, Fe-BC demonstrated a remarkable superiority over RBC in both adsorptive and oxidative remediation strategies. The adsorptive capacity of Fe-BC was significantly higher, achieving a notable LFX final LFX concentration of 335 μg/L within 60 min, while RBC attained a lesser final concentration of 530 μg/L. In the realm of oxidative processes, the performance of Fe-BC was exceptional; the Fe-BC/$S_2O_8^{2-}$ system culminated in a final LFX concentration of merely 2.8 μg/L, a substantial improvement over the 8.9 μg/L achieved by the RBC/$S_2O_8^{2-}$- system. The rapid and efficient removal of LFX by Fe-BC/$S_2O_8^{2-}$ underscores the significant catalytic role played by the iron integration. Furthermore, when coupled with $H_2O_2$, Fe-BC's capability was once again underscored, showing an increase in LFX removal efficiency, measured at 9.5-ln units, and a final LFX concentration of 0.1 μg/L. This is in contrast to the Fe-BC/$S_2O_8^{2-}$ system and even surpasses the efficiency of RBC/$H_2O_2$, which itself performed notably well, showing an efficiency 1-ln unit higher than Fe-BC/$S_2O_8^{2-}$, with a final LFX concentration of 1.2 μg/L. These findings clearly establish the effectiveness of Fe-BC, particularly in conjunction with $H_2O_2$, in purifying water from LFX, and present a compelling case for its application in environmental remediation. Fe-BC/$H_2O_2$ exhibited rapid kinetics, removing 50 % of LFX in the first 2 min and reaching a plateau in just 20 min, emphasizing the catalytic effect of Fe loading. The characterization of degradation by-products provided valuable information on the transformation of LFX during the oxidation process. The results of this study underscore the significance of advanced oxidation processes in addressing the challenges associated with the presence of pharmaceutical compounds in wastewater. The use of Fe-BC as a sustainable catalyst for environmental remediation has the potential to reduce the environmental impact of antibiotic residues in wastewater, especially in scenarios where efficient and rapid removal of contaminants is paramount. Further research is needed to optimize the use of advanced oxidation processes for the degradation of antibiotics in wastewater and to evaluate the potential of iron-modified BC as a catalyst for other environmental remediation applications.

## CRediT authorship contribution statement

**Antonio Faggiano:** Writing – original draft, Methodology, Formal analysis. **Oriana Motta:** Writing – review & editing, Supervision, Conceptualization. **Maurizio Carotenuto:** Methodology, Formal analysis. **Maria Ricciardi:** Writing – review & editing, Formal analysis. **Antonino Fiorentino:** Writing – review & editing, Supervision, Project administration, Conceptualization. **Antonio Proto:** Supervision, Funding acquisition, Conceptualization.

## Declaration of competing interest

The authors declare that they have no known competing financial interests or personal relationships that could have appeared to influence the work reported in this paper.

## Data availability

Data will be made available on request.

## Acknowledgement

This work was funded by the "SyngaSmart 4.0" project (CUP: B49J23000320005) in collaboration with the University of Salerno and the RESET Company (Rome, Italy). The authors thank the RESET (Rome, Italy) Company for supplying the raw biochar.

## Supplementary materials

Supplementary material associated with this article can be found, in the online version, at doi:10.1016/j.ceja.2024.100602.

## References

[1] A. Fiorentino, G. De Luca, L. Rizzo, G. Viccione, G. Lofrano, M. Carotenuto, Simulating the fate of indigenous antibiotic resistant bacteria in a mild slope wastewater polluted stream, J. Environ. Sci. 69 (2018) 95–104, https://doi.org/10.1016/j.jes.2017.04.018.

[2] L. Rizzo, C. Manaia, C. Merlin, T. Schwartz, C. Dagot, M.C. Ploy, I. Michael, D. Fatta-Kassinos, Urban wastewater treatment plants as hotspots for antibiotic resistant bacteria and genes spread into the environment: a review, Sci. Total. Environ. 447 (2013) 345–360, https://doi.org/10.1016/j.scitotenv.2013.01.032.

[3] A.A.P. Khan, A. Khan, A.M. Asiri, S.A. Khan, Studies on the oxidation of levofloxacin by N-bromosuccinimide in acidic medium and their mechanistic pathway, J. Mol. Liq. 218 (2016) 604–610, https://doi.org/10.1016/j.molliq.2016.02.051.

[4] C.-K. Tsai, Y.-C. Lee, T.T. Nguyen, J.-J. Horng, Levofloxacin degradation under visible-LED photo-catalyzing by a novel ternary Fe–ZnO/WO3 nanocomposite, Chemosphere 298 (2022) 134285, https://doi.org/10.1016/j.chemosphere.2022.134285.

[5] X. Van Doorslaer, J. Dewulf, H. Van Langenhove, K. Demeestere, Fluoroquinolone antibiotics: an emerging class of environmental micropollutants, Sci. Total Environ. 500–501 (2014) 250–269, https://doi.org/10.1016/j.scitotenv.2014.08.075.

[6] V.-A. Thai, V.D. Dang, N.T. Thuy, B. Pandit, T.-K.-Q. Vo, A.P. Khedulkar, Fluoroquinolones: fate, effects on the environment and selected removal methods, J. Clean. Prod. 418 (2023) 137762, https://doi.org/10.1016/j.jclepro.2023.137762.

[7] A.M. Franklin, C. Williams, D.M. Andrews, J.E. Watson, Sorption and desorption behavior of four antibiotics at concentrations simulating wastewater reuse in agricultural and forested soils, Chemosphere 289 (2022) 133038, https://doi.org/10.1016/j.chemosphere.2021.133038.

[8] F. Bu, W. Huang, M. Xian, X. Zhang, F. Liang, X. Liu, X. Sun, D. Feng, Magnetic carboxyl-functionalized covalent organic frameworks for adsorption of quinolones with high capacities, fast kinetics and easy regeneration, J. Clean. Prod. 336 (2022) 130485, https://doi.org/10.1016/j.jclepro.2022.130485.

[9] M.J. Stapleton, A.J. Ansari, F.I. Hai, Antibiotic sorption onto microplastics in water: a critical review of the factors, mechanisms and implications, Water Res. 233 (2023) 119790, https://doi.org/10.1016/j.watres.2023.119790.

[10] A.E.D. Mahmoud, M. Fawzy, Decontamination of levofloxacin from water using a novel chitosan–walnut shells composite: linear, nonlinear, and optimization modeling, Appl. Water. Sci. 13 (2023) 244, https://doi.org/10.1007/s13201-023-02045-7.

[11] P. Ding, H. Ji, P. Li, Q. Liu, Y. Wu, M. Guo, Z. Zhou, S. Gao, W. Xu, W. Liu, Q. Wang, S. Chen, Visible-light degradation of antibiotics catalyzed by titania/zirconia/graphitic carbon nitride ternary nanocomposites: a combined experimental and theoretical study, Appl. Catal. B Environ. 300 (2022) 120633, https://doi.org/10.1016/j.apcatb.2021.120633.

[12] A. Fiorentino, G. Lofrano, R. Cucciniello, M. Carotenuto, O. Motta, A. Proto, L. Rizzo, Disinfection of roof harvested rainwater inoculated with E. coli and enterococcus and post-treatment bacterial regrowth: conventional vs solar driven advanced oxidation processes, Sci. Total Environ. 801 (2021) 149763, https://doi.org/10.1016/j.scitotenv.2021.149763.

[13] A. Fiorentino, P. Soriano-Molina, M.J. Abeledo-Lameiro, I. de la Obra, A. Proto, M. I. Polo-López, J.A.S. Pérez, L. Rizzo, Neutral (Fe3+-NTA) and acidic (Fe2+) pH solar photo-Fenton Vs chlorination: effective urban wastewater disinfection does not mean control of antibiotic resistance, J. Environ. Chem. Eng. 10 (2022) 108777, https://doi.org/10.1016/j.jece.2022.108777.

[14] E.A. Serna-Galvis, A.C. Cáceres-Peña, R.A. Torres-Palma, Elimination of representative fluoroquinolones, penicillins, and cephalosporins by solar photo-Fenton: degradation routes, primary transformations, degradation improvement by citric acid addition, and antimicrobial activity evolution, Environ. Sci. Pollut. Res. 27 (2020) 41381–41393, https://doi.org/10.1007/s11356-020-10069-8.

[15] W. Huang, F. Wang, N. Qiu, X. Wu, C. Zang, A. Li, L. Xu, Enteromorpha prolifera-derived Fe3C/C composite as advanced catalyst for hydroxyl radical generation

and efficient removal for organic dye and antibiotic, J. Hazard. Mater. 378 (2019) 120728, https://doi.org/10.1016/j.jhazmat.2019.06.005.
[16] Y. Wang, X. Zhu, D. Feng, A.K. Hodge, L. Hu, J. Lü, J. Li, Biochar-supported FeS/Fe3O4 composite for catalyzed Fenton-type degradation of ciprofloxacin, catalysts 9 (2019) 1062. https://doi.org/10.3390/catal9121062.
[17] Q. Mao, Y. Zhou, Y. Yang, J. Zhang, L. Liang, H. Wang, S. Luo, L. Luo, P. Jeyakumar, Y.S. Ok, M. Rizwan, Experimental and theoretical aspects of biochar-supported nanoscale zero-valent iron activating H2O2 for ciprofloxacin removal from aqueous solution, J. Hazard. Mater. 380 (2019) 120848, https://doi.org/10.1016/j.jhazmat.2019.120848.
[18] G. Chen, Y. Yu, L. Liang, X. Duan, R. Li, X. Lu, B. Yan, N. Li, S. Wang, Remediation of antibiotic wastewater by coupled photocatalytic and persulfate oxidation system: a critical review, J. Hazard. Mater. 408 (2021) 124461, https://doi.org/10.1016/j.jhazmat.2020.124461.
[19] J. Rodríguez-Chueca, E. Laski, C. García-Cañibano, M.J. Martín de Vidales, Á. Encinas, B. Kuch, J. Marugán, Micropollutants removal by full-scale UV-C/sulfate radical based advanced oxidation processes, Sci. Total Environ. 630 (2018) 1216–1225, https://doi.org/10.1016/j.scitotenv.2018.02.279.
[20] M. Pirsaheb, H. Hossaini, H. Janjani, Reclamation of hospital secondary treatment effluent by sulfate radicals based–advanced oxidation processes (SR-AOPs) for removal of antibiotics, Microchem. J. 153 (2020) 104430, https://doi.org/10.1016/j.microc.2019.104430.
[21] A. Faggiano, M. Ricciardi, A. Fiorentino, R. Cucciniello, O. Motta, L. Rizzo, A. Proto, Combination of foam fractionation and photo-Fenton like processes for greywater treatment, Sep. Purif. Technol. 293 (2022) 121114, https://doi.org/10.1016/j.seppur.2022.121114.
[22] F. Sang, Z. Yin, W. Wang, E. Almatrafi, Y. Wang, B. Zhao, J. Gong, C. Zhou, C. Zhang, G. Zeng, B. Song, Degradation of ciprofloxacin using heterogeneous Fenton catalysts derived from natural pyrite and rice straw biochar, J. Clean. Prod. 378 (2022) 134459, https://doi.org/10.1016/j.jclepro.2022.134459.
[23] J. He, J. Tang, Z. Zhang, L. Wang, Q. Liu, X. Liu, Magnetic ball-milled FeS@biochar as persulfate activator for degradation of tetracycline, Chem. Eng. J. 404 (2021) 126997, https://doi.org/10.1016/j.cej.2020.126997.
[24] F. Shao, Y. Wang, Y. Mao, T. Shao, J. Shang, Degradation of tetracycline in water by biochar supported nanosized iron activated persulfate, Chemosphere 261 (2020) 127844, https://doi.org/10.1016/j.chemosphere.2020.127844.
[25] L. Zhang, Y. Guo, R. Xie, L. Chen, W. Jiang, X. Jiang, An efficient catalytic composite material of mesoporous carbon loaded nano zero-valent iron as an activator for the degradation of sulfadiazine, Water Air Soil Pollut. 231 (2020) 375, https://doi.org/10.1007/s11270-020-04709-5.
[26] L. Kemmou, Z. Frontistis, J. Vakros, I.D. Manariotis, D. Mantzavinos, Degradation of antibiotic sulfamethoxazole by biochar-activated persulfate: factors affecting the activation and degradation processes, Catal. Today 313 (2018) 128–133, https://doi.org/10.1016/j.cattod.2017.12.028.
[27] P.V. Nidheesh, A. Gopinath, N. Ranjith, A. Praveen Akre, V. Sreedharan, M. Suresh Kumar, Potential role of biochar in advanced oxidation processes: a sustainable approach, Ch. Eng. J. 405 (2021) 126582, https://doi.org/10.1016/j.cej.2020.126582.
[28] D. Huang, Y. Wang, C. Zhang, G. Zeng, C. Lai, J. Wan, L. Qin, Y. Zeng, Influence of morphological and chemical features of biochar on hydrogen peroxide activation: implications on sulfamethazine degradation, RSC. Adv. 6 (2016) 73186–73196, https://doi.org/10.1039/C6RA11850J.
[29] J. Yan, L. Han, W. Gao, S. Xue, M. Chen, Biochar supported nanoscale zerovalent iron composite used as persulfate activator for removing trichloroethylene, Bioresour. Technol. 175 (2015) 269–274, https://doi.org/10.1016/j.biortech.2014.10.103.
[30] M. Arellano, M. Pazos, M.Á. Sanromán, Sulfate radicals-based technology as a promising strategy for wastewater, Water (Basel) 11 (2019) 1695, https://doi.org/10.3390/w11081695.
[31] F. Ghanbari, M. Moradi, Application of peroxymonosulfate and its activation methods for degradation of environmental organic pollutants: review, Chem. Eng. J. 310 (2017) 41–62, https://doi.org/10.1016/j.cej.2016.10.064.
[32] M.I. Litter, M. Slodowicz, An overview on heterogeneous Fenton and photoFenton reactions using zerovalent iron materials, J. Adv. Oxid. Technol. 20 (2017), https://doi.org/10.1515/jaots-2016-0164.
[33] J. Li, L. Pan, G. Yu, S. Xie, C. Li, D. Lai, Z. Li, F. You, Y. Wang, The synthesis of heterogeneous Fenton-like catalyst using sewage sludge biochar and its application for ciprofloxacin degradation, Sci. Total Environ. 654 (2019) 1284–1292, https://doi.org/10.1016/j.scitotenv.2018.11.013.
[34] K.K. Rubeena, P. Hari Prasad Reddy, A.R. Laiju, P.V. Nidheesh, Iron impregnated biochars as heterogeneous Fenton catalyst for the degradation of acid red 1 dye, J. Environ. Manage. 226 (2018) 320–328, https://doi.org/10.1016/j.jenvman.2018.08.055.
[35] J. Deng, H. Dong, C. Zhang, Z. Jiang, Y. Cheng, K. Hou, L. Zhang, C. Fan, Nanoscale zero-valent iron/biochar composite as an activator for Fenton-like removal of sulfamethazine, Sep. Purif. Technol. 202 (2018) 130–137, https://doi.org/10.1016/j.seppur.2018.03.048.
[36] H.-A.S. Tohamy, M. El-Sakhawy, S. Kamel, Microwave-assisted synthesis of amphoteric fluorescence carbon quantum dots and their chromium adsorption from aqueous solution, Sci. Rep. 13 (2023) 11306, https://doi.org/10.1038/s41598-023-37894-4.
[37] T. Sizmur, T. Fresno, G. Akgül, H. Frost, E. Moreno-Jiménez, Biochar modification to enhance sorption of inorganics from water, Bioresour. Technol. 246 (2017) 34–47, https://doi.org/10.1016/j.biortech.2017.07.082.
[38] R. Cai, X. Wang, X. Ji, B. Peng, C. Tan, X. Huang, Phosphate reclaim from simulated and real eutrophic water by magnetic biochar derived from water hyacinth, J. Environ. Manage. 187 (2017) 212–219, https://doi.org/10.1016/j.jenvman.2016.11.047.
[39] X. Hu, Z. Ding, A.R. Zimmerman, S. Wang, B. Gao, Batch and column sorption of arsenic onto iron-impregnated biochar synthesized through hydrolysis, Water Res. 68 (2015) 206–216, https://doi.org/10.1016/j.watres.2014.10.009.
[40] D. Mohan, H. Kumar, A. Sarswat, M. Alexandre-Franco, C.U. Pittman, Cadmium and lead remediation using magnetic oak wood and oak bark fast pyrolysis biochars, Chem. Eng. J. 236 (2014) 513–528, https://doi.org/10.1016/j.cej.2013.09.057.
[41] L. Trakal, V. Veselská, I. Šafařík, M. Vítková, S. Číhalová, M. Komárek, Lead and cadmium sorption mechanisms on magnetically modified biochars, Bioresour. Technol. 203 (2016) 318–324, https://doi.org/10.1016/j.biortech.2015.12.056.
[42] W. Tang, Y. Zhang, H. Guo, Y. Liu, Heterogeneous activation of peroxymonosulfate for bisphenol AF degradation with BiOI0.5Cl0.5, RSC. Adv. 9 (2019) 14060–14071, https://doi.org/10.1039/C9RA01687B.
[43] Y.-H. Jo, S.-H. Do, S.-H. Kong, Persulfate activation by iron oxide-immobilized MnO2 composite: identification of iron oxide and the optimum pH for degradations, Chemosphere 95 (2014) 550–555, https://doi.org/10.1016/j.chemosphere.2013.10.010.
[44] C. Liang, C.-F. Huang, N. Mohanty, R.M. Kurakalva, A rapid spectrophotometric determination of persulfate anion in ISCO, Chemosphere 73 (2008) 1540–1543, https://doi.org/10.1016/j.chemosphere.2008.08.043.
[45] A. Faggiano, M. Ricciardi, O. Motta, A. Fiorentino, A. Proto, Greywater treatment for reuse: effect of combined foam fractionation and persulfate-iron based Fenton process in the bacterial removal and degradation of organic matter and surfactants, J. Clean. Prod. 415 (2023) 137792, https://doi.org/10.1016/j.jclepro.2023.137792.
[46] A. Fiorentino, G. Ferro, M.C. Alferez, M.I. Polo-López, P. Fernández-Ibañez, L. Rizzo, Inactivation and regrowth of multidrug resistant bacteria in urban wastewater after disinfection by solar-driven and chlorination processes, J. Photochem. Photobiol. B Biol. 148 (2015) 43–50, https://doi.org/10.1016/j.jphotobiol.2015.03.029.
[47] P.V. Nidheesh, R. Gandhimathi, Comparative removal of rhodamine b from aqueous solution by electro-fenton and electro-Fenton-like processes, clean – soil, Air Water 42 (2014) 779–784, https://doi.org/10.1002/clen.201300093.
[48] P. Godlewska, A. Bogusz, J. Dobrzyńska, R. Dobrowolski, P. Oleszczuk, Engineered biochar modified with iron as a new adsorbent for treatment of water contaminated by selenium, J. Saudi Chem. Soc. 24 (2020) 824–834, https://doi.org/10.1016/j.jscs.2020.07.006.
[49] A. Faggiano, O. Motta, M. Ricciardi, F. Cerrato, C.A. Garcia Junior, A. Fiorentino, A. Proto, Integrated anaerobic–aerobic moving bed biofilm reactor and biochar adsorption for the efficient removal of organic matter and nutrients from Brazilian landfill leachate, Sustainability 15 (2023) 13914.
[50] B. Peng, L. Chen, C. Que, K. Yang, F. Deng, X. Deng, G. Shi, G. Xu, M. Wu, Adsorption of antibiotics on graphene and biochar in aqueous solutions induced by π-π interactions, Sci. Rep. 6 (2016) 31920, https://doi.org/10.1038/srep31920.
[51] U. Sen, B. Esteves, T. Aguiar, H. Pereira, Removal of antibiotics by Biochars: a critical review, Appl. Sci. 13 (2023) 11963, https://doi.org/10.3390/app132111963.
[52] L.O. Conte, J. Farias, E.D. Albizzati, O.M. Alfano, Photo-fenton degradation of the herbicide 2,4-dichlorophenoxyacetic acid in laboratory and solar pilot-plant reactors, Ind. Eng. Chem. Res. 51 (2012) 4181–4191, https://doi.org/10.1021/ie2023228.
[53] B.N. Giménez, L.O. Conte, F. Audino, A.V. Schenone, M. Graells, O.M. Alfano, M. Pérez-Moya, Kinetic model of photo-Fenton degradation of paracetamol in an annular reactor: main reaction intermediates and cytotoxicity studies, Catal. Today 413–415 (2023) 113958, https://doi.org/10.1016/j.cattod.2022.11.019.
[54] J.J. Pignatello, E. Oliveros, A. MacKay, Advanced oxidation processes for organic contaminant destruction based on the Fenton reaction and related chemistry, Crit. Rev. Environ. Sci. Technol. 36 (2006) 1–84, https://doi.org/10.1080/10643380500326564.
[55] M. Simunovic, H. Kusic, N. Koprivanac, A.L. Bozic, Treatment of simulated industrial wastewater by photo-Fenton process: part II. The development of mechanistic model, Chem. Eng. J. 173 (2011) 280–289, https://doi.org/10.1016/j.cej.2010.09.030.
[56] H. Kusic, I. Peternel, S. Ukic, N. Koprivanac, T. Bolanca, S. Papic, A.L. Bozic, Modeling of iron activated persulfate oxidation treating reactive azo dye in water matrix, Chem. Eng. J. 172 (2011) 109–121, https://doi.org/10.1016/j.cej.2011.05.076.
[57] N. Kang, D.S. Lee, J. Yoon, Kinetic modeling of Fenton oxidation of phenol and monochlorophenols, Chemosphere 47 (2002) 915–924, https://doi.org/10.1016/S0045-6535(02)00067-X.
[58] E. Gualda-Alonso, P. Soriano-Molina, J.L. García Sánchez, J.L. Casas López, J. A. Sánchez Pérez, Mechanistic modeling of solar photo-Fenton with Fe3+-NTA for microcontaminant removal, Appl. Catalysis B Environ. 318 (2022) 121795, https://doi.org/10.1016/j.apcatb.2022.121795.
[59] R.F.F. Pontes, J.E.F. Moraes, A. Machulek, J.M. Pinto, A mechanistic kinetic model for phenol degradation by the Fenton process, J. Hazard. Mater. 176 (2010) 402–413, https://doi.org/10.1016/j.jhazmat.2009.11.044.
[60] B. Yao, Z. Luo, S. Du, J. Yang, D. Zhi, Y. Zhou, Sustainable biochar/MgFe2O4 adsorbent for levofloxacin removal: adsorption performances and mechanisms, Bioresour. Technol. 340 (2021) 125698, https://doi.org/10.1016/j.biortech.2021.125698.
[61] Z. Wan, J. Wang, Degradation of sulfamethazine using Fe3O4-Mn3O4/reduced graphene oxide hybrid as Fenton-like catalyst, J. Hazard. Mater. 324 (2017) 653–664, https://doi.org/10.1016/j.jhazmat.2016.11.039.

[62] M. Wang, Y. Wang, Y. Li, C. Wang, S. Kuang, P. Ren, B. Xie, Persulfate oxidation of tetracycline, antibiotic resistant bacteria, and resistance genes activated by Fe doped biochar catalysts: synergy of radical and non-radical processes, Chem. Eng. J. 464 (2023) 142558, https://doi.org/10.1016/j.cej.2023.142558.
[63] Y. Yao, L. Wang, L. Sun, S. Zhu, Z. Huang, Y. Mao, W. Lu, W. Chen, Efficient removal of dyes using heterogeneous Fenton catalysts based on activated carbon fibers with enhanced activity, Chem. Eng. Sci. 101 (2013) 424–431, https://doi.org/10.1016/j.ces.2013.06.009.
[64] Z. Cheng, S. Li, T.T. Nguyen, X. Gao, S. Luo, M. Guo, Biochar loaded on MnFe2O4 as Fenton catalyst for Rhodamine B removal: characterizations, catalytic performance, process optimization and mechanism, Coll. Surf. A: Physicochem. Eng. Asp. 631 (2021) 127651, https://doi.org/10.1016/j.colsurfa.2021.127651.
[65] C. Wang, R. Huang, R. Sun, Green one-spot synthesis of hydrochar supported zero-valent iron for heterogeneous Fenton-like discoloration of dyes at neutral pH, J. Mol. Liq. 320 (2020) 114421, https://doi.org/10.1016/j.molliq.2020.114421.
[66] N. Thomas, D.D. Dionysiou, S.C. Pillai, Heterogeneous Fenton catalysts: a review of recent advances, J. Hazard. Mater. 404 (2021) 124082, https://doi.org/10.1016/j.jhazmat.2020.124082.
[67] S. Navalon, A. Dhakshinamoorthy, M. Alvaro, H. Garcia, Heterogeneous Fenton catalysts based on activated carbon and related materials, ChemSusChem. ChemSusChem. 4 (2011) 1712–1730, https://doi.org/10.1002/cssc.201100216.
[68] C. Wang, R. Jiang, J. Yang, P. Wang, Enhanced heterogeneous fenton degradation of organic pollutants by CRC/Fe3O4 catalyst at neutral pH, Front Chem 10 (2022). https://www.frontiersin.org/article/10.3389/fchem.2022.892424. accessed June 9, 2022.
[69] I. Epold, N. Dulova, Oxidative degradation of levofloxacin in aqueous solution by S2O82−/Fe2+, S2O82−/H2O2 and S2O82−/OH− processes: a comparative study, J. Environ. Chem. Eng. 3 (2015) 1207–1214, https://doi.org/10.1016/j.jece.2015.04.019.
[70] L. Foti, D. Coviello, A. Zuorro, F. Lelario, S.A. Bufo, L. Scrano, A. Sauvetre, S. Chiron, M. Brienza, Comparison of sunlight-AOPs for levofloxacin removal: kinetics, transformation products, and toxicity assay on Escherichia coli and micrococcus flavus, Environ. Sci. Pollut. Res. 29 (2022) 58201–58211, https://doi.org/10.1007/s11356-022-19768-w.
[71] H. Wei, D. Hu, J. Su, K. Li, Intensification of levofloxacin sono-degradation in a US/H2O2 system with Fe3O4 magnetic nanoparticles, Chin. J. Chem. Eng. 23 (2015) 296–302, https://doi.org/10.1016/j.cjche.2014.11.011.
[72] M.Sh. Yahya, M.El Karbane, N. Oturan, K. El Kacemi, M.A. Oturan, Mineralization of the antibiotic levofloxacin in aqueous medium by electro-Fenton process: kinetics and intermediate products analysis, Environ .Technol. 37 (2016) 1276–1287, https://doi.org/10.1080/09593330.2015.1111427.
[73] Y. Gong, J. Li, Y. Zhang, M. Zhang, X. Tian, A. Wang, Partial degradation of levofloxacin for biodegradability improvement by electro-Fenton process using an activated carbon fiber felt cathode, J. Hazard. Mater. 304 (2016) 320–328, https://doi.org/10.1016/j.jhazmat.2015.10.064.
[74] X. Lin, Y. Ma, Y. Wang, J. Wan, Z. Guan, Lithium iron phosphate (LiFePO4) as an effective activator for degradation of organic dyes in water in the presence of persulfate, RSC. Adv. 5 (2015) 94694–94701, https://doi.org/10.1039/C5RA19697C.
[75] G. Fang, J. Gao, C. Liu, D.D. Dionysiou, Y. Wang, D. Zhou, Key role of persistent free radicals in hydrogen peroxide activation by biochar: implications to organic contaminant degradation, Environ. Sci. Technol. 48 (2014) 1902–1910, https://doi.org/10.1021/es4048126.
[76] E. Elmolla, M. Chaudhuri, Optimization of Fenton process for treatment of amoxicillin, ampicillin and cloxacillin antibiotics in aqueous solution, J. Hazard. Mater. 170 (2009) 666–672, https://doi.org/10.1016/j.jhazmat.2009.05.013.
[77] E.S. Elmolla, M. Chaudhuri, The feasibility of using combined Fenton-SBR for antibiotic wastewater treatment, Desalination 285 (2012) 14–21, https://doi.org/10.1016/j.desal.2011.09.022.
[78] S. Dehghani, A. Jonidi Jafari, M. Farzadkia, M. Gholami, Sulfonamide antibiotic reduction in aquatic environment by application of fenton oxidation process, J. Environ. Health Sci. Eng. 10 (2013) 29, https://doi.org/10.1186/1735-2746-10-29.
[79] A. Leovac Maćerak, A. Kulić Mandić, V. Pešić, D. Tomašević Pilipović, M. Bečelić-Tomin, D. Kerkez, Green" nZVI-Biochar as fenton catalyst: perspective of closing-the-loop in wastewater treatment, Molecules 28 (2023) 1425, https://doi.org/10.3390/molecules28031425.